Anders Teigmoen

# Harmonic Resonance Analysis of Offshore Wind Farm utilizing Type-IV Wind Turbines

Master's thesis in Energy and Environmental Engineering
Supervisor: Kjetil Uhlen
Co-supervisor: Kamran Sharifabadi

June 2021

**Master's thesis**

**NTNU**
Norwegian University of Science and Technology
Faculty of Engineering
Department of Electric Power Engineering

**NTNU**
Norwegian University of
Science and Technology

Anders Teigmoen

# Harmonic Resonance Analysis of Offshore Wind Farm utilizing Type-IV Wind Turbines

Master's thesis in Energy and Environmental Engineering
Supervisor: Kjetil Uhlen
Co-supervisor: Kamran Sharifabadi
June 2021

Norwegian University of Science and Technology
Faculty of Engineering
Department of Electric Power Engineering

**NTNU**
Norwegian University of
Science and Technology

# Abstract

To achieve the sustainable development goals set by the UN, the utilization of renewable energy sources are of paramount importance. Of these energy sources, offshore wind has a substantial potential. To utilize this potential, offshore wind farms have to increase in size. With an expansion of the offshore collector grid, the length of subsea cables and the number of transformers and power electronic devices increase. This presents system operators with two interweaved challenges. The first is the fact that power electronic devices, such as converters, affect the power system dynamics and stability. The other challenge is that cables, transformers and wind turbine generators introduce more capacitance and inductance to a system, which lowers the resonance frequency of the respective system.

The dynamic between a lowered resonance frequency and increased number of power electronic devices may cause stability issues in weak AC grids, such as offshore collector grids. This lays the foundation for Harmonic Resonance Analysis, which can be used to investigate the impedance interaction between the installed converters and the grid. Although, a substantial challenge related to Harmonic Resonance Analysis is the need for impedance representations of the grid and converter. The control structure and parameter values of the converters affect its frequency response. Therefore, in order to get an accurate impedance model of the respective converters, full insight into the controller is necessary. Although, this is not disclosed information by the manufacturers of the converters due to intelligence property.

In this thesis, the Harmonic Resonance Analysis technique named Current/Voltage Perturbation Technique is successfully used on an offshore wind farm model, utilizing Type-IV turbines, in PSCAD. This technique reveals the frequency response of the collector grid and the grid-side converter. The technique enables inclusion of the dynamic behavior of the converter, without having the knowledge of the controller structure. The issue related to converter manufacturers not revealing intelligence property can therefore be resolved by implementing this Harmonic Resonance Analysis technique.

Once the converter- and grid impedances are derived, the interaction between the two are analyzed. It is revealed that, depending on the difference in phase angles, the intersection between the magnitudes of the converter- and grid impedances results in an equivalent resonance frequency. In addition, by comparing a single-string wind farm to that of a 100-string wind farm, it is found that the expansion of the collector grid reduces the first equivalent parallel resonance between the converter- and grid impedances. For the single-string wind farm, the first equivalent parallel resonance frequency is found to occur at 710 Hz. Although, when the number of strings are increased to 100, the corresponding resonance frequency occurs at 280 Hz. This implies that the stability regions of a system is heavily dependent on the system topology. The possible interactions between converter impedances and different system topologies is therefore discussed. Consequently, this thesis fortifies the need for Harmonic Resonance Analysis.

The impact of control parameters on the converter frequency response is then examined. This is attempted by introducing time delays into the current controller on the grid-side converter. Unfortunately, no change in impedance is registered. The time delay should have resulted in

frequency ranges where negative damping is exhibited by the converter. If a resonance frequency coincides with a negatively damped frequency range, the system stability would be further worsened. The most probable reason for the failed attempt is the use of an already existing controller model made by PSCAD.

When unstable frequency ranges are revealed to a system operator, it may be of interest to mitigate the discovered resonances and potential negative damping effects. As a consequence, possible implementable measures, such as passive and active filters, are presented in this thesis and the merits of each option is discussed.

# Sammendrag

Utnyttelse av fornybare energikilder er av største betydning for å oppnå de bærekraftige utviklingsmålene som er satt av FN. Av disse energikildene har havvind et betydelig potensiale. For å utnytte dette potensialet må vindparker til havs øke i størrelse. Med en utvidelse av offshore kollektornettet øker lengden på havkabler og antall transformatorer og kraftelektroniske enheter. Dette gir systemoperatører to sammenvevde utfordringer. Den første utfordringen er det faktum at kraftelektroniske enheter, som omformere, påvirker kraftsystemets dynamikk og stabilitet. Den andre er at kabler, transformatorer og vindturbingeneratorer introduserer mer kapasitans og induktans til et system, noe som senker resonansfrekvensen til det respektive systemet.

Dynamikken mellom senket resonansfrekvens og økt antall kraftelektroniske enheter kan forårsake stabilitetsproblemer i svake AC-nett, for eksempel offshore-kollektor-nett. Dette legger grunnlaget for Harmonisk Resonansanalyse som kan brukes til å undersøke impedansinteraksjonen mellom de installerte omformerne og nettet. Dog, en betydelig utfordring knyttet til harmonisk resonansanalyse er behovet for impedansrepresentasjoner for nettet og omformeren. Kontrollstrukturen og parameterverdiene til omformerne påvirker frekvensresponsen. Derfor, for å få en nøyaktig impedansmodell for de respektive omformerne, er full innsikt i kontrolleren nødvendig. Dog, dette er ikke utlevert informasjon fra produsentene av omformerne på grunn av etterretningseiendom.

Denne avhandlingen beskriver forskjellige metoder interessenter i kraftsystemet kan bruke for å utføre Harmonisk Resonansanalyse. En av disse metodene, nemlig Voltage/Current Perturbation Technique, blir vellykket brukt på en offshore vindparkmodell, modellert med Type- IV turbiner, i PSCAD. Teknikken muliggjør utledning av frekvensresponsen til omformeren uten å ha kjennskap til kontrollerstrukturen.

Når omformer- og nettimpedansene er utledet, blir samspillet mellom de to analysert. Det er avdekket at, avhengig av forskjellen i fasevinkler, skjæringspunktet mellom størrelsen på omformer- og nettimpedansene resulterer i en ekvivalent resonansfrekvens. I tillegg er det funnet, ved å sammenligne en enkeltstrenget vindpark med en 100-strenget vindpark, at utvidelsen av kollektornettet reduserer den første ekvivalente parallelle resonansen mellom omformer- og nettimpedansene. For en enstrengs vindpark er den første ekvivalente parallelle resonansfrekvensen funnet å forekomme ved 710 Hz. Om antall strenger økes til 100, forekommer den korresponderende resonansfrekvensen ved 280 Hz. Dette tilsier at stabilitetsregionene til et system er sterkt avhengig av systemtopologien. De mulige samspillene mellom omformerimpedanser og forskjellige systemtopologier blir derfor diskutert. Denne oppgaven understreker dermed behovet for Harmonisk Resonansanalyse.

Virkningen av kontrollparametere på omformerens frekvensrespons blir deretter undersøkt. Dette forsøkes ved å innføre tidsforsinkelser i strøm-kontrolleren på omformeren som ligger på nettsiden. Dessverre er ingen endring i impedanse registrert. Tidsforsinkelsen skulle ha resultert i frekvensområder der omformeren viser negativ demping. Hvis en resonansfrekvens sammenfaller med et negativt dempet frekvensområde, vil systemstabiliteten bli ytterligere forverret. Den mest sannsynlige årsaken til det mislykkede forsøket er bruken av en allerede eksisterende

kontrollermodell laget av PSCAD.

Når ustabile frekvensområder avdekkes for en systemoperatør, kan det være av interesse å redusere de oppdagede resonansene og potensielle negative dempningseffektene. Som en konsekvens presenteres mulige implementerbare tiltak, som passive og aktive filtre, i denne oppgaven, og fordelene ved hvert alternativ blir diskutert.

# Preface

This Master's Thesis was completed in the Spring of 2021 at the Department of Electrical Power Engineering in the Master's-program Energy- and Environmental Engineering at The Norwegian University of Science and Technology (NTNU). The project is equivalent to 30 ECT credits.

Lastly, I would like to thank myself. There have been many ups and downs since I started my time as a student at NTNU, but giving up was never an option. It is also worth mentioning that the last year at NTNU has been heavily influenced by COVID-19, so to still achieve this makes me proud.

Trondheim, June 28th 2021

Anders Teigmoen

# Nomenclature

$\Delta V_{\text{DC}}$    Voltage ripple [V]

$\hat{V}_{\text{o1}}$      Peak fundamental frequency output voltage [V]

$|I_{\text{fund}}|$   Magnitude of fundamental current [A]

$|I_{\text{h}}|$     Magnitude of $h$th-order harmonic current [A]

$\omega_0$      Angular frequency at fundamental frequency [rad/s]

$\omega_{\text{sw}}$     Angular frequency at switching frequency [rad/s]

$\theta_{\text{PLL}}$    PLL output angle [rad]

$A_{\text{core}}$   Area of transformer core [m$^2$]

$B_{\text{sat}}$    Saturation flux density [$W/m^2$]

$f_r$       Resonance frequency [Hz]

$H_d$      Control delay transfer function

$H_{wi}$     Current controller transfer function

$H_{wv}$    Voltage controller transfer function

$N$        Number of turns [-]

$P$        Number of pulses [-]

$X$        Reactance [$\Omega$]

$Z$        Impedance [$\Omega$]

$Z_c$       Filter impedance

$Z_{\text{HVDC}}$   VSC-HVDC Impedance

C        Capacitance [F]

C$_{\text{damp}}$   Damping capacitance [F]

C$_{\text{DC}}$    DC-link capacitance [F]

C$_{\text{filter}}$   Filter capacitance [F]

$C_I$       Transfer function of current control loop

$C_V$       Transfer function of voltage control loop

f       Frequency [Hz]

$f_f$       Fundamental frequency [Hz]

$f_{cutoff}$       Cutoff frequency [Hz]

$f_{sw}$       Switching frequency [Hz]

I       Current [A]

$I_0$       Current, Zero-sequence [A]

$I_1$       Current, Positive-sequence [A]

$I_2$       Current, Negative-sequence [A]

$I_a$       Current, Phase a [A]

$I_b$       Current, Phase b [A]

$I_{conv}$       Current flowing towards converter [A]

$I_c$       Current, Phase c [A]

$I_{d,error}$       d-axis current error [pu]

$I_{d,ord}$       d-axis current order [pu]

$I_d$       d-axis current [pu]

$I_{grid}$       Current flowing towards grid [A]

$I_{inject}$       Injected current [V]

$I_i$       Current at bus i [A]

$I_{nom,peak\text{-}to\text{-}peak}$       Peak-to-peak nominal current [A]

$I_{nom}$       Nominal current [A]

$I_{q,error}$       q-axis current error [pu]

$I_{q,ord}$       q-axis current order [pu]

$I_q$       q-axis current [pu]

$I_{ripple}$       Ripple current [A]

$I_{rpp}$       Ripple current [A]

$I_r$       DC-link current [A]

$K_i$       Integral gain

$K_p$      Proportional gain

$L$      Inductance [H]

$L_{damp}$      Damping inductance [H]

$L_{inv}$      Converter inductance [H]

$m_a$      Modulation index [-]

$P$      Watt [W]

$P_{conv}$      Watt [W]

$Q$      Reactive Power [VAr]

$Q_{error}$      Reactive power error [pu]

$Q_{measure}$      Measured reactive power [pu]

$R$      Resistance [$\Omega$]

$R_{damp}$      Damping resistance [$\Omega$]

$T_i$      Integral time

$THD_I$      Total Harmonic Distortion of current signal [%]

$THD_V$      Total Harmonic Distortion of voltage signal [%]

$V$      Voltage [V]

$V_0$      Voltage, Zero-sequence [V]

$V_1$      Voltage, Positive-sequence [V]

$V_2$      Voltage, Negative-sequence [V]

$V_a$      Voltage, Phase a [V]

$V_b$      Voltage, Phase b [V]

$V_c$      Voltage, Phase c [V]

$V_{d,ref}$      d-axis voltage reference [pu]

$V_{DC,base}$      Base DC-voltage [kV]

$V_{DC,error}$      DC-voltage error [pu]

$V_{DC}$      DC-Voltage [V]

$V_d$      d-axis voltage [pu]

$V_{error}$      Voltage error [pu]

$V_{inject}$      Injected voltage [V]

$V_i$      Voltage at bus i [V]

$V_{\text{L-L rms}}$ Line-to-line RMS Voltage [V]

$V_{\text{PCC}}$    Voltage at PCC [V]

$V_{\text{PEH}}$    Voltage drop caused by power electronic hardware

$V_{q,\text{ref}}$    q-axis voltage reference [pu]

$V_q$      q-axis voltage [pu]

$V_{\text{ref}}$     Voltage reference [pu]

$V_{\text{rms,ref}}$ RMS reference voltage value [pu]

$V_{s,d}$     Supplied DC voltage [pu]

$V_{\text{Synth}}$ Reference voltage synthesizing

$Z_1$      Positive sequence impedance [$\Omega$]

$Z_2$      Negative sequence impedance [$\Omega$]

$Z_{\text{conv}}$   Impedance of converter [$\Omega$]

$Z_{\text{eq}}$     Equivalent impedance [$\Omega$]

$Z_{\text{grid}}$    Impedance of grid [$\Omega$]

$Z_{\text{ii}}$      Driving impedance [$\Omega$]

# Abbreviations

| | |
|---|---|
| AC | Alternating Current |
| DC | Direct Current |
| HRMA | Harmonic Resonance Mode Analysis |
| OWF | Offshore Wind Farm |
| PMSG | Permanent Magnet Synchronous Generator |
| PLL | Phase-Locked Loop |
| PWM | Pulse-Width Modulation |
| MMC | Modular Multilevel Converter |
| HVDC | High-Voltage Direct Current |
| HVAC | High-Voltage Alternating Current |
| LFAC | Low-Frequency Alternating Current |
| SSMA | State-Space Modal Analysis |
| WTG | Wind Turbine Generator |
| THD | Total Harmonic Distortion |
| VSC | Voltage Source Converter |
| LCC | Line-Communtating Converter |
| IGBT | Insulated Gate Bipolar Transistor |
| SVC | Static VAr Compensators |
| STATCOM | Static Synchronous Compensator |
| PCC | Point of Common Coupling |
| EMT | Electromagnetic Transient |
| IPR | Intellectual Property |
| RMS | Root-Mean Square |
| EMT | Electromagnetic Transient |

# Contents

# List of Figures

# List of Tables

# Chapter 1

# Introduction

## 1.1  Problem Background and Motivation for Research

To utilize the vast potential of offshore wind energy, Offshore Wind Farms (OWFs) must increase in size. As the distribution system is increased, the interarray cables are getting longer and more transformers are installed. This leads to a more capacitive and inductive grid. Together with the Wind Turbine Generators (WTGs), this capacitance and inductance creates a LC circuit. This increase in capacitance and inductance makes the resonance frequency of the grid to drop. If the circuit is excited by harmonics within the area of this resonance frequency, this could lead to peaks in voltages and currents, which could further trip the protection system and possibly damage system components. Additionally, the power electronic converters in the offshore grid further affect the frequency response of the system because of its control systems. The system integrator is responsible for the system's function. This underlines the necessity of proper Harmonic Resonance Analysis to ensure the functionality of the system.

In order to perform Harmonic Resonance Analysis, an accurate impedance representation of the respective system is detriment to the quality of the results. Therefore, knowledge of the control system's structure and parameter values is necessary, which leads to a major challenge - this information is not disclosed by the manufacturers of the power electronic converters since it is often considered as Intellectual Property (IPR). This thesis investigates how a system integrator can derive the frequency response of the installed converter, explains the interaction between the converter- and grid impedances, investigates how the converter controller impacts the converter impedance and discusses possible measures to mitigate the problems associated with the discovered resonances. The control parameter in focus is the effect of time delays within the current controller. According to literature, the presence of time delays causes the converter to exhibit negative damping in certain frequency ranges. If a resonance frequency coincides with a frequency with negative damping, continuous emission of the harmonic components located within this resonance is the result. Consequently, unstable operation would ensue and the protection system would trip. This potential interaction demands attention and underlines the need for Harmonic Resonance Analysis.

## 1.2  Project Goals & Limitations of Scope

The objectives of this project are to:

- Investigate the sources of harmonic instability and explain the relevant background theory.
- Describe the different methods the industry can utilize to perform Harmonic Resonance Analysis.

- Use the Voltage/Current Perturbation Technique on an OWF model in PSCAD where Type-IV wind turbines are utilized. This is in order to derive the WTG's converter frequency response.

- Perform Harmonic Resonance Analysis on the converter and OWF. This reveals the interaction between the converter and offshore grid in the form of potential equivalent resonance frequencies.

- Investigate how the converter control parameters affect the converter impedance. The main focus is how time delays in the current controller introduces negative damping in some frequency ranges.

- Discuss possible measures that mitigate the discovered resonances and potential negative damping effects.

There are limitations of this thesis. They are listed below.

- The OWF model is primarily based on existing models from PSCAD's knowledge base. This is especially true for the converter control structure and parameters.

- No analytical equivalent is made of the converter- and grid impedances, which makes the comparative foundation weak.

- Only one Harmonic Resonance Technique is implemented, namely the Voltage/Current Perturbation Technique.

## 1.3   Relation to Specialization Project

The project goals of the Specialization Project were to:

1. provide insight into the background theory related to emission of harmonics and the resonance phenomenon.

2. elaborate on existing sources of harmonics and the effect of harmonic resonance in OWFs. Possible measures to mitigate these issues were also investigated.

3. describe and evaluate different applicable techniques used Harmonic Resonance Analysis in power systems.

This thesis is built on the foundation on the author's Specialization Project. The first point in the list above laid the groundwork for Section 2.2. The second point is the foundation of Sections 1.5 and 2.3. The third point heavily influences Sections 2.5, 4.1 and partly 4.2.

This thesis is also a substantial extension on what was accomplished in the Specialization Project. Since no actual simulations or analysis were performed in that project, contrary to in this thesis, Section 4.2 is recognized as a continuation of previous work. There, the method that finds itself in the center of attention in this thesis is explained.

## 1.4   Structure of Thesis

In Chapter 2, the fundamental background theory related to the thesis is explained. This includes symmetrical components, harmonics and resonances. The terms passive and active impedance, together with harmonic instability, are introduced. Additionally, a literature study of how control parameters affect converter impedance is performed.

To be able to perform a Harmonic Resonance Analysis, a working model is essential. Chapter 3 covers how the Type-IV wind turbine is modeled and connected to the onshore grid by HVAC transmission. The model can be adjusted to being either a single string containing the wind turbine and collection grid or an aggregated model, which can represent several strings connected to a Point of Common Coupling (PCC).

Chapter 4 builds on the Specialization Project of the author, [1], and describes different methods that can be used in deriving the system and/or converter impedance. The main focus is on the Current/Voltage Perturbation Technique.

In Chapter 5, the results from applying the method described in Section 4.2 on the model is presented. This includes the frequency response of the isolated converter and the frequency response of the overall grid together with the converter. Additionally, a verification model where the frequency response is analyzed analytically and compared to the numerical results of the same model.

Chapter 6 discusses the positive and negative aspects of the approach. Sources of error and possible factors affecting the quality of the results are elaborated on.

Lastly, the conclusions are presented in Chapter 7 and ideas for further work are proposed.

## 1.5   Offshore Transmission Technologies

In this section, the different transmission technologies, both applied and researched, are explained and evaluated. The current status and future outlook of offshore transmission is discussed.

### 1.5.1   High-Voltage Alternating Current

High-Voltage Alternating Current (HVAC) is the most common transmission technology used in OWFs. This is due to the simple and economical technology utilized in the connection between the OWF and the onshore grid. The offshore collector grid is usually at a voltage level of 33 kV before it is stepped up to transmission level, e.g. 220 kV, in an offshore substation. The main components in an HVAC OWF are listed below and illustrated in figure 1.5.1.[2, 3]

- Wind turbines constituting an offshore wind farm

- Offshore substation

- Reactive power compensators

- Three-core crosslinked polyethylene (XLPE) cables

- Onshore substation
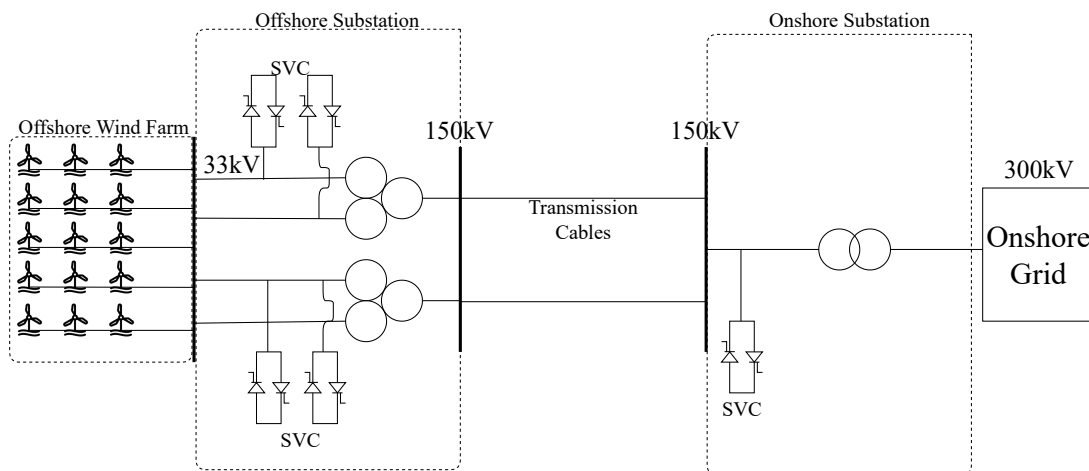


**Figure 1.5.1:** Illustration of a typical HVAC schematic. The figure is from [3, 4]

Despite being the most applied transmission technology, HVAC has it's shortcomings. For OWFs that are situated at a far distance from shore, dependent on the power transfer capacity of the cables, the power losses are considered ineligible. In addition, reactive power compensation devices are needed at both ends of the line because of the long distance. Furthermore, because of the synchronous coupling between the farm and the onshore grid, a fault on any side would affect the other side, which could result in serious consequences. As the distribution system is increased, the interarray cables are getting longer and more transformers are installed. This leads to a more capacitive and inductive grid. Together with the WTGs, this capacitance and inductance creates a LC circuit. This increase in capacitance and inductance makes the global resonance frequency of the grid to drop. If a fault on the onshore grid occurs, this could lead to harmonic currents that coincides with this resonance frequency. Consequently, oscillations would occur, the protection system would trip and equipment might get damaged. Lastly, the high capacitance may deteriorate the voltage shape.[2, 3]

As mentioned in [2, 3, 5, 6], an example of a HVAC solution is the wind farm Horns Rev 1 in Denmark. It is located approximately 21 km from shore and is rated at 160 MW. No reactive

power compensation is needed at the offshore transformer station because of the relative short distance. The farm consists of 80 Vestas V80 turbines, each rated at $2\,\mathrm{MW}$, situated in an area with water depths equal to 10 meters.

### 1.5.2   Low-Frequency Alternating Current

To increase the possible transmission length, Low-Frequency Alternating Current (LFAC) can be implemented. This is a transmission technology that applies lower frequencies. This is revealed by investigating equations 1.5.1 and 1.5.2, which are expressions for transmission capacity and voltage drop, respectively.[2, 3]

$$P_{\mathrm{max}} = \frac{V^2}{X} \tag{1.5.1}$$

$$\Delta V\% = \frac{QX}{V^2} \cdot 100\% \tag{1.5.2}$$

V is the transmission voltage, X is the reactance of the transmission line and Q is the reactive power flow. By studying the equations, it is observed that the transmission capability can be increased by increasing the transmission voltage or by decreasing the reactance. Furthermore, the reactance is proportional to the inductance and frequency, as shown in equation 1.5.3.[3]

$$X = 2\pi f L \tag{1.5.3}$$

As a consequence, by lowering the frequency, the reactance also decreases. This results in an increase in transmission capability and a decrease in voltage drop. In addition to increasing the transmission capability, a decrease in frequency allows for a less complicated design of the generator. The rotor revolves slowly in large turbines, which creates the demand for a gearbox with a large gear ratio. The generator could be direct driven or the gear ratio could be substantially reduced with a lower AC frequency. Consequently, the wind turbine is lighter and may be less expensive.[2, 3]

A possible structure of an LFAC system is presented in figure 1.5.2. A wind turbine is depicted as a generator that generates power at a low frequency. In this case, the chosen frequency is $50/3\,\mathrm{Hz}$. The voltage is then stepped up in a transformer, situated in an offshore substation, before it is transmitted to the onshore substation. The frequency is then converted into the utility grid's respective frequency by a frequency converter, eg. a matrix converter, back-to-back converter or a cycloconverter, and the voltage is stepped down to utility level by an onshore transformer.[2, 3]
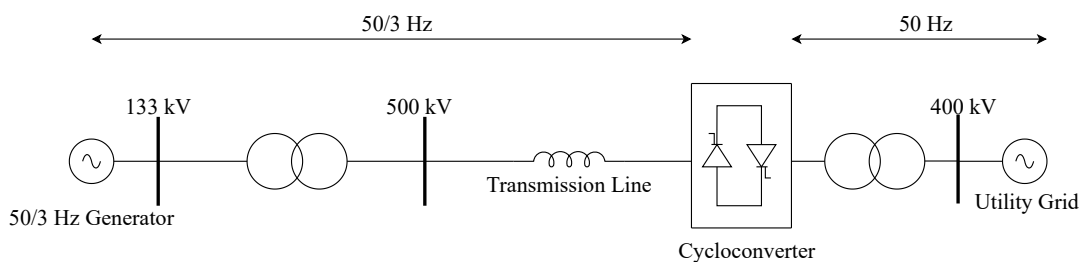


**Figure 1.5.2:** Illustration of a typical LFAC transmission system. The figure is from [2, 3]

Decreasing the transmission frequency has it's negative aspects related to the offshore transformer. The area of the transformer core is calculated by applying equation 1.5.4. V is the

applied voltage, f is the frequency, N is the number of turns and $B_{sat}$ is the material's saturation flux density.[2, 3]

$$A_{\text{core}} \approx \frac{V}{4.44fNB_{\text{sat}}} \tag{1.5.4}$$

When the frequency is decreased, it is observed that the area of the core in the transformer increases. This, in turn, increases the cost of the transformer. According to [3, 5], LFAC transmission systems for offshore wind farms are not being pursued by the industry.

### 1.5.3   High-Voltage Direct Current

High-Voltage Direct Current (HVDC) transmission systems applies direct current at high voltages to transmit power from the offshore wind farm to the onshore grid. Power is transmitted from the OWF at 33 kV by medium-voltage alternating current (MVAC) cables to an offshore AC substation where the voltage is stepped up to HVAC. The power is transmitted further to an offshore HVDC substation. It is then transferred by HVDC cables to an onshore substation. Converting from HVAC to to HVDC can be accomplished by utilizing one of two technologies: Line-Commutated Converter (LCC) or Self-Commutated Voltage Source Converter (VSC). These two technologies are further reviewed in this section. [2–4]

**LCC**

Figure 1.5.3 is an illustration of a LCC-HVDC transmission system. The LCC is based on thyristors, has a high power rating and use mass-impregnated cables. Consequently, it is suitable for transmitting large bulks of power over great distances. Although, it requires strong AC grids on both sides of the converter stations and has a large footprint. This makes LCC-HVDC an unsuitable configuration for offshore power transmission. According to [3, 5], there is no experience in the utilization of HVDC based on line-commutated converters in transmission from OWFs because of this. On the other hand, with the use of reactive power compensation equipment, such as a static synchronous compensator (STATCOM), a LCC-HVDC scheme may attain similar attributes related to the reactive power control and voltage regulation as in a VSC-HVDC scheme. This means that LCC-HVDC can be a suitable configuration for remote onshore wind farms [3, 7].
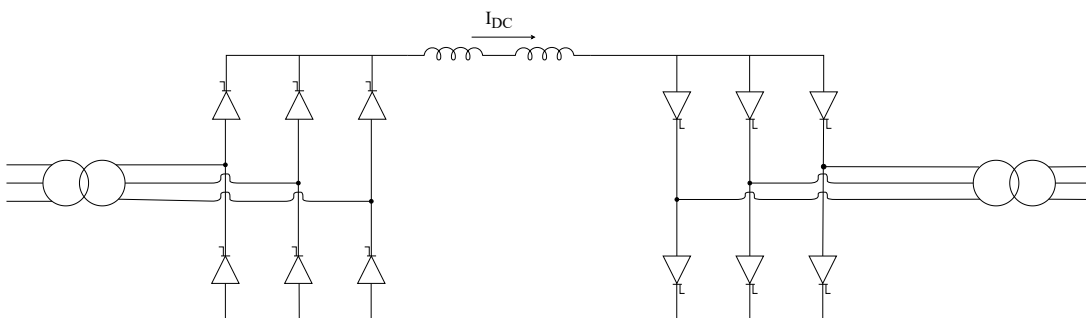


**Figure 1.5.3:** Illustration of a LCC-HVDC system. The figure is from [3, 8]

**VSC**

An illustration of a VSC-HVDC transmission system is displayed in figure 1.5.4. The VSC is based on Insulated Gate Bipolar Transistors (IGBTs), which are gates that can be turned on and off by injecting a pulse. This provides the possibility of applying Pulse-Width Modulation
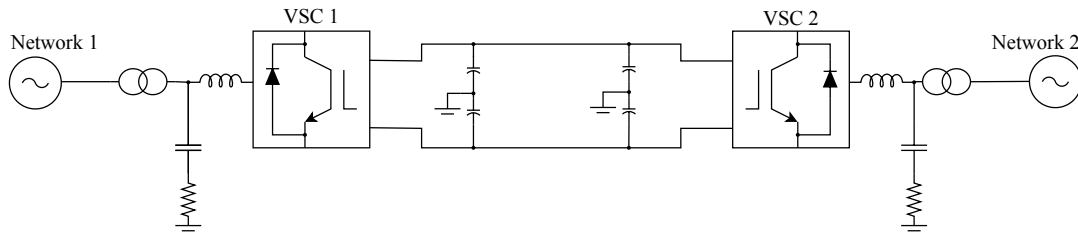
**Figure 1.5.4:** Illustration of a VSC-HVDC system. The figure is based on [2, 3]

(PWM). It also enables performing a black start and controlling active and reactive power flow. [2–4].

The configuration of the VSC is composed of different components. The series inductors between the transformers and converter reduce high-frequency harmonic current components and controls the active and reactive power flow. The DC-link capacitors are used as energy storage units, reduce the DC voltage ripple and control the power flow. [3, 4]

The OWFs Veja Mate, Global Tech 1 and Albatros are all examples of existing VSC-HVDC scheme. They are all connected to the offshore HVDC converter platform BorWin2. The network connection is 200 km long and has a capacity of 800 MW. The total number of turbines connected are 163, with 67 6 MW SWT-6.0-154 turbines at Veja Mate, 80 5 MW AREVA M5000-116 turbines at Global Tech 1 and 16 7 MW Siemens Gamesa SWT-7.0-154 turbines at Albatros. [3, 9–12]

VSCs can have different topologies, such as two-level, three-level and multilevel. The number of levels indicate how many levels the output voltage can have. Figure 1.5.5 illustrates a circuit for a single phase of a two-level converter. The two-level VSC generates an output voltage of either $\frac{1}{2}V_{DC}$ or $-\frac{1}{2}V_{DC}$ between the point 'a' and the middle of the DC capacitor. This is possible by using the switching scheme Pulse-Width Modulation. PWM enables regulating the magnitude and phase angle of the output AC voltage and is the applied technique for two-level, three-level and multilevel converters.The lower number of voltage levels, the higher switching frequency is utilized. This means that between the different converters, the two-level has the highest switching frequency. Additionally, the relationship between switching frequency and switching losses are proportional. Lastly, for low amount of voltage levels, the converter transformer experiences large DC voltage steps.Consequently, it has to be able to withstand high-voltage stress. [3, 4]

Following the logic of the previous paragraph, the three-level VSC has lower switching losses and the converter transformer experiences lower voltage stress. This is due to the lower switching frequency of the converter and that the output voltage can be at three levels. The possible levels are $\frac{1}{2}V_{DC}$, 0 and $-\frac{1}{2}V_{DC}$. There are four different design topologies for a three-level VSC; neutral point clamped, T-type, active neutral point clamped and hybrid neutral point clamped. An illustration of a single phase of a neutral point clamped converter is displayed in figure 1.5.6. [3, 4]
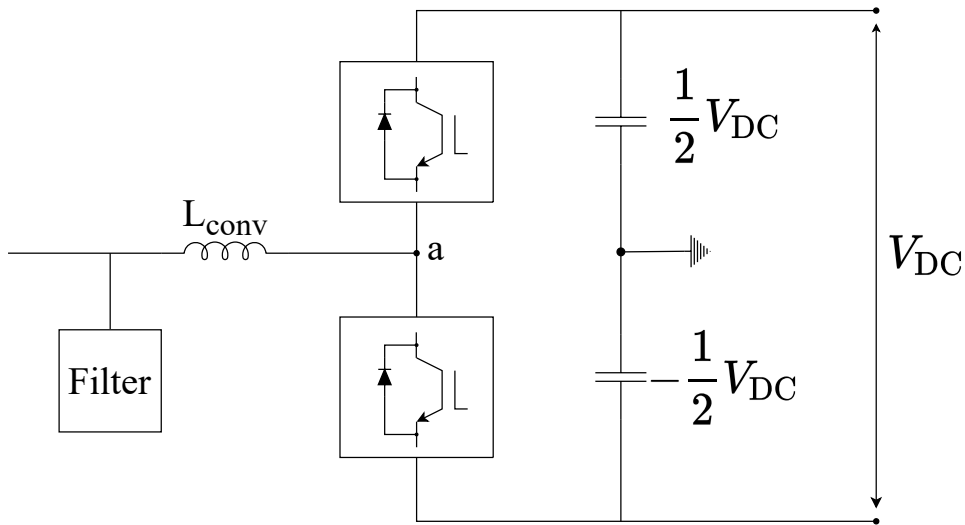
**Figure 1.5.5:** Illustration of a two-level VSC. The figure is based of [3, 4]
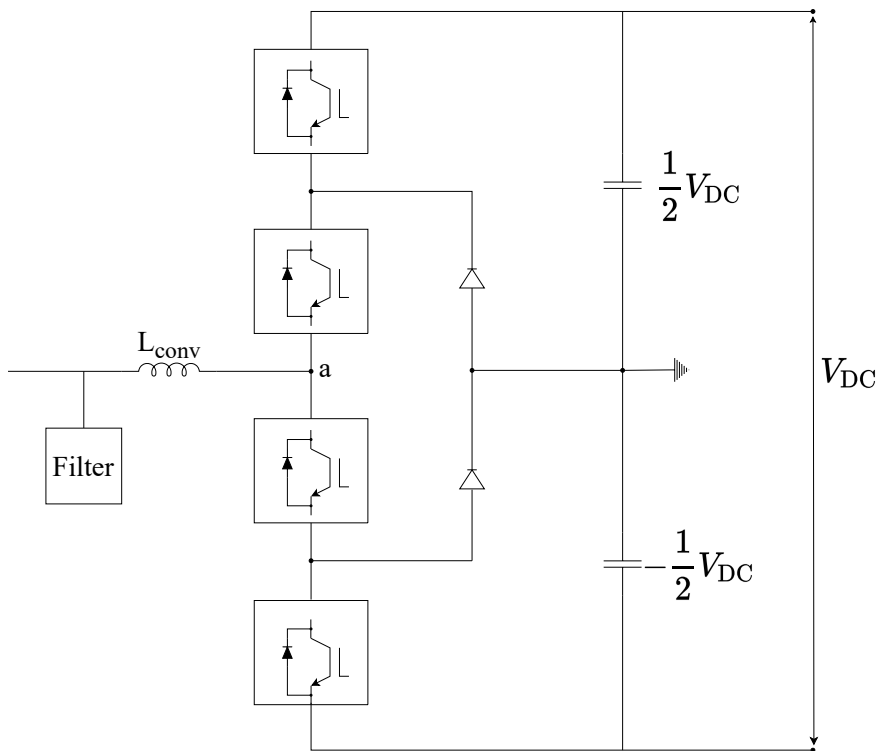


**Figure 1.5.6:** Illustration of a three-level neutral point clamped VSC. The figure is from [3, 4]

Lastly, the multilevel VSC converter is able to switch between multiple voltage levels. Consequently, it enables operation with even lower switching frequency than the two- and three-level converters. Because of this, it is more efficient, emits less harmonic components and the transformer does not experience high DC voltage stresses. Figure 1.5.7 displays one of two designs for a multilevel VSC, namely the Modular Multilevel Converter (MMC). The MMC consists of three phase arms, where each consists of two multivalve arms. Each multivalve arm further consists of multiple submodules, which are connected in series with an arm reactor. The submodules comprise of a DC capacitor, IGBTs and diodes. The purpose of the series reactor is to smooth the phase currents and limit the circulating currents during unbalanced operation and limit the inrush current during voltage balancing of the capacitor. [3, 4]
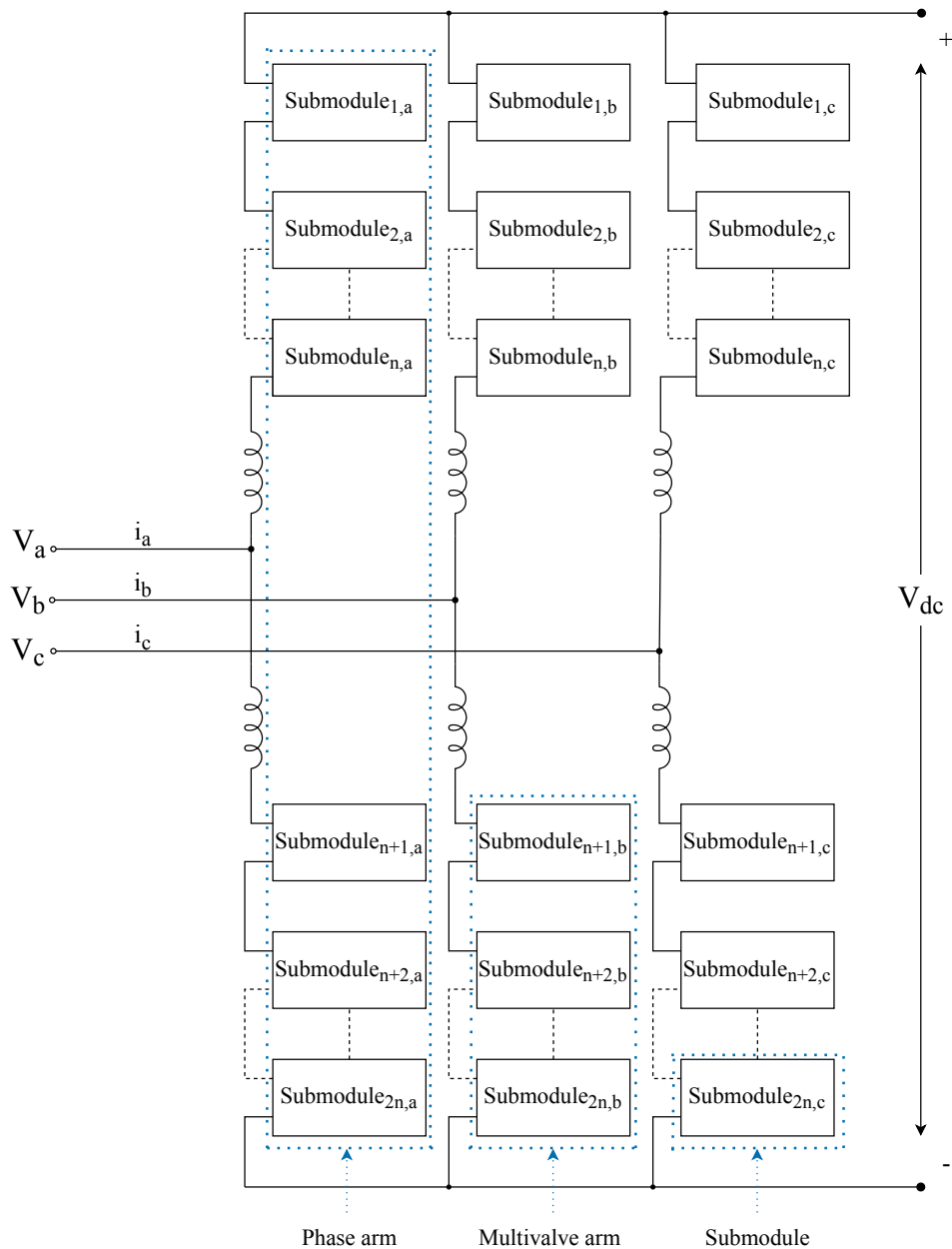


**Figure 1.5.7:** Illustration of a modular multilevel VSC. The figure is from [3].

# Chapter 2

# Theoretical background

## 2.1 Symmetrical Components

To simplify analysis of unbalanced power systems, Charles Legeyt Fortescue discovered the method of applying symmetrical components. This method involves expressing three phase voltages or currents into the following three sets of sequence components:

1. *Zero-sequence* - consisting of three phasors with 0° displacement and equal magnitude. Shown in figure 2.1.1 a) [13].

2. *Positive-sequence* - consisting of three phasors with ± 120° displacement, equal magnitude and the same phase sequence as the investigated system (eg. ABC). Shown in figure 2.1.1 b) [13].

3. *Negative-sequence* - consisting of three phasors with ± 120° displacement, equal magnitude and the reverse phase sequence as the investigated system (eg. ACB). Shown in figure 2.1.1 c) [13].
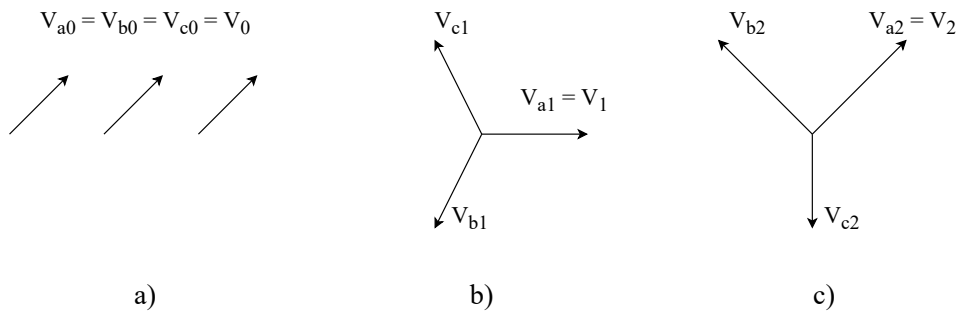


**Figure 2.1.1:** Illustration of the different symmetrical components. a) Zero-sequence, b) Positive-sequence, c) Negative-sequence. [13]

Moving forward in this thesis, only phase $a$ is worked with. With this in mind, the subscript $a$ is denoted. The transformation from phase values to symmetrical components is given by the following equation:

$$\begin{bmatrix} V_a \\ V_b \\ V_c \end{bmatrix} = \begin{bmatrix} 1 & 1 & 1 \\ 1 & a^2 & a \\ 1 & a & a^2 \end{bmatrix} \begin{bmatrix} V_0 \\ V_1 \\ V_2 \end{bmatrix} = \mathbf{A} \begin{bmatrix} V_0 \\ V_1 \\ V_2 \end{bmatrix}$$

In the above equation, $a$, located in the **A**-matrix, is a complex number with unit magnitude and a phase angle of 120°, shown in equation 2.1.1. Consequently, $a^2$ has a unit magnitude and a phase angle of 240°, shown in equation 2.1.2.

$$a = 1\underline{/120°} \qquad (2.1.1)$$

$$a^2 = 1\underline{/240°} \qquad (2.1.2)$$

The inverse of the **A**-matrix is:

$$\mathbf{A}^{-1} = \tfrac{1}{3} \cdot \begin{bmatrix} 1 & 1 & 1 \\ 1 & a & a^2 \\ 1 & a^2 & a \end{bmatrix}$$

This is used when calculating the symmetrical components from phase values, as shown below.

$$\begin{bmatrix} V_0 \\ V_1 \\ V_2 \end{bmatrix} = \tfrac{1}{3} \cdot \begin{bmatrix} 1 & 1 & 1 \\ 1 & a & a^2 \\ 1 & a^2 & a \end{bmatrix} \begin{bmatrix} V_a \\ V_b \\ V_c \end{bmatrix}$$

This can further be written as three separate equations, shown in equations 2.1.3, 2.1.4 and 2.1.5.

$$V_0 = \frac{1}{3}\left(V_a + V_b + V_c\right) \qquad (2.1.3)$$

$$V_1 = \frac{1}{3}\left(V_a + aV_b + a^2V_c\right) \qquad (2.1.4)$$

$$V_2 = \frac{1}{3}\left(V_a + a^2V_b + aV_c\right) \qquad (2.1.5)$$

By studying equation 2.1.3 it becomes apparent that in a balanced system there is no zero-sequence component. This is due to the sum of the three balanced phasors is zero. Symmetrical components are not only used for voltages, but also currents. The calculation is the exact same, as shown below.

$$\begin{bmatrix} I_0 \\ I_1 \\ I_2 \end{bmatrix} = \tfrac{1}{3} \cdot \begin{bmatrix} 1 & 1 & 1 \\ 1 & a & a^2 \\ 1 & a^2 & a \end{bmatrix} \begin{bmatrix} I_a \\ I_b \\ I_c \end{bmatrix}$$

Equations 2.1.6, 2.1.7 and 2.1.8 show how the separated equations look.

$$I_0 = \frac{1}{3}\left(I_a + I_b + I_c\right) \qquad (2.1.6)$$

$$I_1 = \frac{1}{3}\left(I_a + aI_b + a^2I_c\right) \qquad (2.1.7)$$

$$I_2 = \frac{1}{3}\left(I_a + a^2I_b + aI_c\right) \qquad (2.1.8)$$

## 2.2   Harmonics & Resonances in Power Systems

This section explains the fundamental theory related to what harmonic components and resonance frequencies are, how they are measured and how they affect power systems. In addition, the relation between voltage- and current harmonics is elaborated on.

### 2.2.1   Harmonics

The supplied electricity to a point of connection should have a sinusoidal waveform. Because of the increased application of power electronics such as converters, categorized as non-linear loads, this requirement has become more challenging to uphold. This is due to the non-linear loads emitting harmonic components, which distorts the sinusoidal waveform. This waveform distortion is explained as harmonic distortion. The harmonics themselves are sinusoidal voltages and currents with a frequency that is an integer multiple of the fundamental frequency. The fundamental frequency is equal to the utility frequency of the given power system. Equation 2.2.1 is an expression for the harmonic frequency. [1, 14–16]

$$f_h = h \cdot f_f \tag{2.2.1}$$

The $f_h$ is the harmonic frequency, $h$ is the order of the harmonic and $f_f$ is the fundamental frequency. Voltages and currents with a frequency below the fundamental frequency, i.e. $h < 1$, are called subharmonics. In the case where voltages and currents have a frequency that is a multiple of the fundamental frequency and a non-integer, the frequency is called interharmonics. [1, 14]

Power quality can be determined by different indices, such as Total Harmonic Distortion (THD). The THD is a measure of the total contribution of the harmonic components to a signal. Equation 2.2.3 is an expression for the total harmonic distortion for a voltage signal, and Equation 2.2.2 is the same for a current signal. The expressions show that the THD is defined as the ratio between the sum of the magnitudes of all harmonics and the magnitude of the fundamental frequency component.[1, 14]

$$\text{THD}_I = \frac{\sqrt{\sum_{h=2}^{\infty} I_h^2}}{I_1} \tag{2.2.2}$$

$$\text{THD}_V = \frac{\sqrt{\sum_{h=2}^{\infty} V_h^2}}{V_1} \tag{2.2.3}$$

To quantify the harmonics of a signal, fourier analysis can be used. It is a method used in the time domain to reveal the magnitude and phase of each harmonic component of a periodic waveform. The Fourier series of a function $f(t)$ is given by Equation 2.2.4. [1, 17]

$$f(t) = a_0 + \sum_{n=1}^{\infty} \left( a_n cos \left( \frac{2\pi n t}{T} \right) + b_n sin \left( \frac{2\pi n t}{T} \right) \right) \tag{2.2.4}$$

The coefficients $a_0$, $a_n$ and $b_n$ are expressed as Equations 2.2.5, 2.2.6 and 2.2.7, respectively. The period is given as $L$. [1, 18]

$$a_0 = \frac{1}{L} \int_0^L f(t) \, dt \tag{2.2.5}$$

$$a_n = \frac{2}{L} \int_0^L f(t) \cos\left(\frac{2\pi n t}{L}\right) dt \tag{2.2.6}$$

$$b_n = \frac{2}{L} \int_0^L f(t) \sin\left(\frac{2\pi n t}{L}\right) dt \tag{2.2.7}$$

In [1], to exemplify the method, a voltage signal of 220 V and a fundamental frequency of 50 Hz was analyzed using Fourier. The result is presented in Figure 2.2.1. By examining the figure, it is observed that the voltage signal contain 3rd, 5th and 7th order harmonic components. This example underlines the effect of harmonics and why they should be mitigated as much as possible.
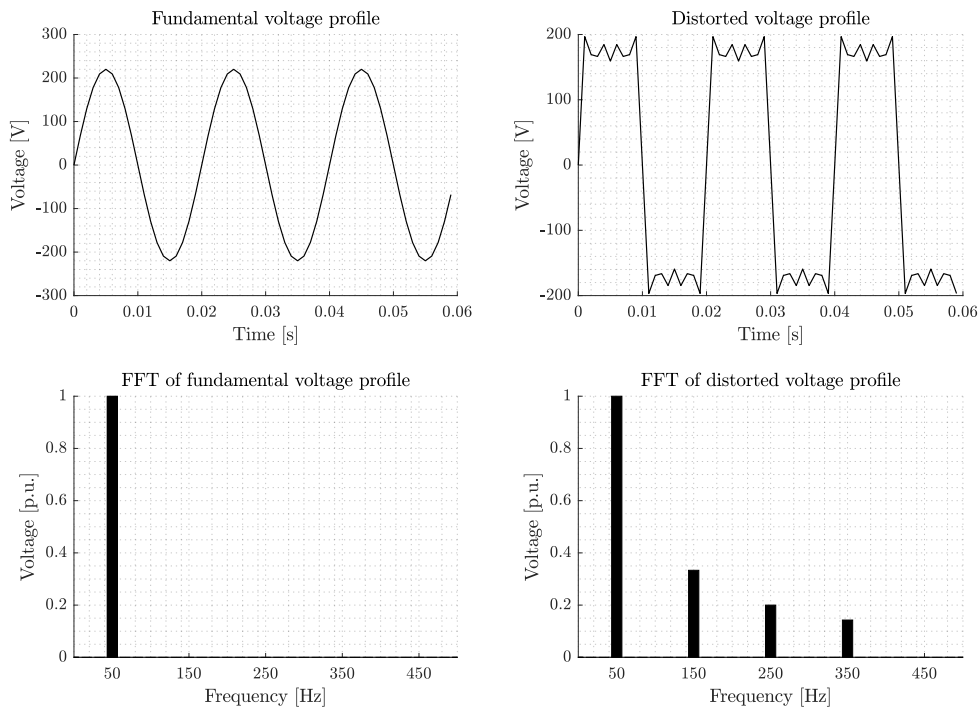


**Figure 2.2.1:** Resulting Fourier analysis of an example voltage signal of 220 V and a fundamental frequency of 50 Hz.

### 2.2.2    Relationship between voltage- and current harmonics

As previously stated, non-linear loads cause the emission of harmonics, more specifically, they act as harmonic current sources. This means that they do not emit voltage harmonics directly. The current harmonics flows through the source and line impedances and creates harmonic voltage drops across these impedances. This results in voltage harmonics and a distorted supply voltage waveform. More sources of impedance in the grid, eg. longer cables and transformers, contribute to higher source of impedance, which in turn results in higher voltage harmonics. [19]

A practical example of why current- and voltage harmonics should be regarded separately is given by [19] where two hypothetical industries, A and B, are given. Industry A has a system containing a high number of non-linear loads and therefore generates a lot of current harmonics. Connected to the same grid, Industry B does not have many non-linear loads, but it experiences high voltage harmonics. The reason for this is the current harmonics emitted by Industry A and the impedance of the grid and transformers. If Industry B implements mitigating measures,

such as power factor correction, due to the introduced capacitors, current harmonics may also appear. This in turn magnifies the voltage harmonics further. [19]

### 2.2.3  Resonance

Inductive and capacitive reactances are dependent on the frequency. This means that for different frequencies, the total reactance of a network is altered. At a certain frequency, the inductive and capacitive reactances become equal. At this frequency, these inductive and capacitive components begin to resonate with each other. This frequency is called the natural frequency, or resonance frequency, of the system. Equation 2.2.8 demonstrates how the resonance frequency is calculated. [1, 16, 20]

$$f_r = \frac{1}{2\pi}\sqrt{\frac{1}{\text{LC}}} \tag{2.2.8}$$

C is the total capacitance and L is the total inductance of the system. If a harmonic component coincides with the resonance frequency, this may lead to an amplification of either the voltage or current. This may lead to unstable operations, tripping of the protection system, damaged or destroyed equipment and potentially dangerous situations. Because of this potential risk, analysis and mitigation of harmonics is important. There are two different types of resonance; parallel and series.[1]

Figure 2.2.2 depicts the equivalent circuits of a) parallel resonance and b) series resonance, including resistances. The impedance is purely resistive and at its maximum for the parallel resonance. Consequently, in the case of a harmonic current, there is an amplification of the voltage. For the series resonance, the impedance is purely resistive and at its minimum. This, in turn, results in high currents. [1, 14]
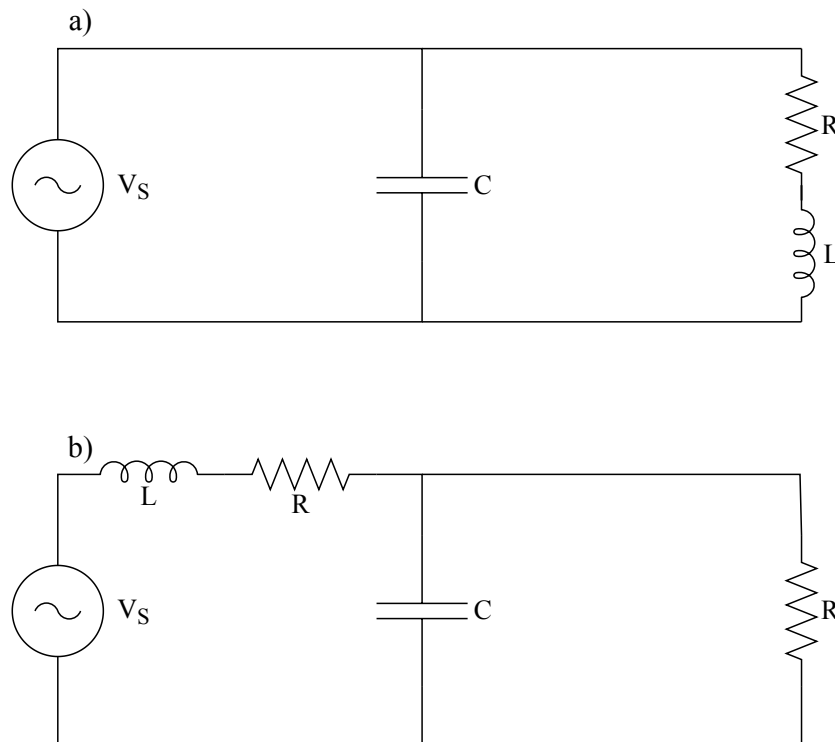


**Figure 2.2.2:** Equivalent circuits of a) parallel- and b) series resonance, including resistances.[1]

## 2.3 Mitigation of Harmonics and Damping of Resonances

Mitigation of harmonics and damping of resonances are essential to reduce the total harmonic distortion of a signal and important for the stability and safe operation of a system. There are several routes to accomplishing this; active- or passive filters can be installed to provide damping and filter out emitted harmonics and the system can be designed to emit lower amounts. This section first elaborates on different filter technologies before moving on to alternative methods of reducing emission of harmonics in the first place.

### 2.3.1 Filter technologies

Filters utilize techniques that can be divided into three main categories; passive, active and hybrid. Passive filters use passive elements, like resistances, inductors and capacitors. The resistor provides the damping to the system, while the inductor and capacitor minimize the active power losses and filters out the predefined harmonics. Active filters use components such as fast-switching IGBTs within their circuit. In addition, they are connected to an external power source in order to boost the output signal. A hybrid filter utilizes both passive and active elements in its design. [1, 21, 22]

**Passive filters**

There are many different types of passive filters. In this thesis, three topologies are elaborated on - the notch filter and two LCL filters; i) standard C-type topology and ii) two capacitive branches with a bypass inductor. Common features for all passive filters are the introduction of damping to the system, which is beneficial related to the system stability. If a resonance frequency is discovered, a filter may be designed to minimize the impedance amplitude at the given resonance frequency. It is also possible to design the filter to move the resonance frequency to another frequency. They are also characterized as having high power losses.[23]

The notch filter, illustrated in Figure 2.3.1, is a simple circuit consisting of a series connected resistor, inductor and capacitor. The advantage of the notch filter is its simple design and its ability to do reactive power compensation. On the other hand, it is only possible to tune it to filter out harmonics of one specific frequency. This disadvantage can be worked around by installing several notch filters in parallel, although, this leads to a peak in the magnitude between the frequencies each respective filter is tuned for. In the case of a non-characteristic harmonic coinciding with the peak, this results in an increase in voltage, which may prove harmful to the system.[1, 24, 25]
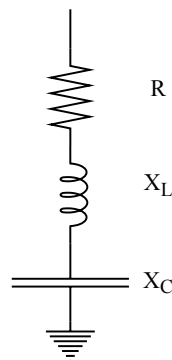


**Figure 2.3.1:** Equivalent circuit of a notch filter. [25]

Figure 2.3.2 depicts the equivalent circuit of the LCL filter with a standard C-type topology. The LCL filter is commonly used as an interconnection between converters and the utility grid because of its ability to smooth the output currents from the converter. In addition, they provide good performance in relation to the small values of inductors and capacitors. The LCL filter also provides higher harmonic attenuation, which allows a lower switching frequency while achieving the harmonic limits set by standards such as IEEE-519 and IEEE-1547 [26]. In the C-type topology, the capacitor and inductor are tuned to the fundamental frequency, resulting in the majority of the fundamental current flowing through them in stead of the resistor. This leads to a reduction in active power losses. Compared to the notch filter, the C-type dampens the notches and has a much larger bandwidth. This results in the mitigation of interharmonic components.[1, 25, 27]
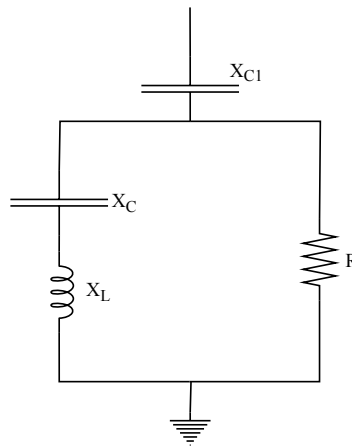


**Figure 2.3.2:** Equivalent circuit of a C-type filter. [1, 25]

Figure 2.3.3 illustrates the LCL filter with two capacitive branches with one bypass inductor. Other topologies can be found in [28]. In this topology, the capacitive branch is split in two. The reason for this is to increase the high frequency attenuation. The inductor is installed in parallel with the resistor in order to reduce the losses at the fundamental frequency. [28]
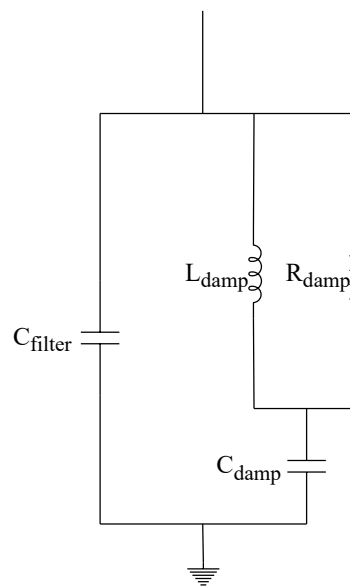


**Figure 2.3.3:** Equivalent circuit of a LCL filter. [28]

**Active filters**

As previously mentioned, active filters utilize IGBTs and external power sources in its design, which can be characterized as active gain elements, hence the name of the filter technology. Due to inductors being considered bulky and expensive in addition to having larger power losses at lower frequencies, the filter only consists of resistors and capacitors [1, 29]. In addition to reactive power compensation, active filters mitigate harmonic components of several orders and provide active damping of resonance frequencies [1, 23, 30]. This means that it can dynamically alter the impedance of the respective system. The disadvantages of such filters are the high cost of the switching devices and limited bandwidth due to time delay when communicating with converters. [1, 23, 31]

**Hybrid filters**

Filters consisting of both active and passive components are categorized as hybrid filters. The aim with these filters are to combine the relative low cost of the passive filters with the high performance of the active filters. [1, 31, 32]

### 2.3.2   System design

As previously stated, converters are large sources of harmonics. One way to reduce the emission of these harmonics is to design the converters with this in mind. According to [33, 34], viable strategies to decrease the harmonic emission is to increase the number of levels and pulses of the converter. This section elaborates more on why this is the case.

Section 1.5.3 explains some of the different converter topologies utilized in offshore power systems, namely the LCC and VSC. The different topologies of the VSC output different voltage levels and affects the harmonic emission of the respective converter. The main factor deciding the harmonic emission is the switching frequency of the converter. For a two-level VSC, the switching frequency has to be high in order to acquire the desired AC-side voltage. Because of the high rate of switching, the converter in turn emits a high number of harmonics. By increasing the number of output voltage levels, the switching frequency can be lowered. For a MMC, for example, since every submodule is not involved in every change in output voltage, the frequency at which the output voltage is changed can be increased without increasing the switching frequency. This results in the emission of harmonics of higher order, which can be more easily filtered out. [1, 34]

The order of harmonics drawn by the converter from the generator also depends on the number of pulses of the converter. This is explained by Equation 2.3.1, where $h$ is the harmonic order, $P$ is the number of pulses in the converter and $n$ is an integer greater than or equal to 1. [1, 33]

$$h = P \cdot n \pm 1 \tag{2.3.1}$$

For a six-pulse converter, the current will have its characteristic harmonic components of the order 5, 7, 11, 13, and so on [1, 33]. The magnitude of each respective harmonic component can be estimated by Equation 2.3.2. $|I_h|$ is the magnitude of the $h$th-order harmonic and $|I_{\text{fund}}|$ is the magnitude of the fundamental current [1, 14]. This means that a high number of pulses in theory results in lower magnitudes of the harmonic components.

$$|I_h| = \frac{|I_{\text{fund}}|}{h} \tag{2.3.2}$$

Another strategy is to use phase-shifting transformers to nullify harmonic currents. In [35], five 12-pulse AC-DC converters are installed in parallel with zigzag-coupled power transformers with

phase shift equal to -12°, -6°, 0°, +6° and +12°. This configuration resulted in an equivalent 60-pulse system, which greatly reduced the magnitude of the harmonic currents [35].

## 2.4 The Effects of Harmonics and Resonances

Since every power system is different, so are the effects of harmonics and resonances. Although, there are common features, which are covered in this section.

If the frequency of a harmonic component of the voltage or current coincides with the resonance frequency, this harmonic component is magnified. This may lead to damaged or destroyed equipment and potentially dangerous situations. Because of this potential risk, analysis of the system's respective resonance frequencies and mitigation of emitted harmonics is important.[1, 14, 16]

Harmonic currents can cause overheating in motors and transformers due to the increased amount of eddy currents and hysteresis losses. Since the harmonic currents increase the RMS current, power losses also increase. Regarding capacitor banks and reactors in transformers, this is associated with breaking down of insulation and failure of internal fuses, all contributing to a decrease in expected lifetime of the component. [1, 16, 19, 36]

Voltage harmonics have a degrading effect on the output voltage signal. This may affect sensitive equipment, like circuit breakers, and may result in difficulty breaking at voltage zero-crossing. [1, 19, 36]

## 2.5 Interaction between Converter and Grid

Consider an offshore grid connected to the MMC-HVDC transmission system illustrated in figure 2.5.1. Once the converter is connected to the system, the impedance of the system is altered. Consequently, the resonance frequency of the system is altered as well. This section elaborates on the impedance contribution of the converter and how the interaction between converters and the grid could lead to resonances.
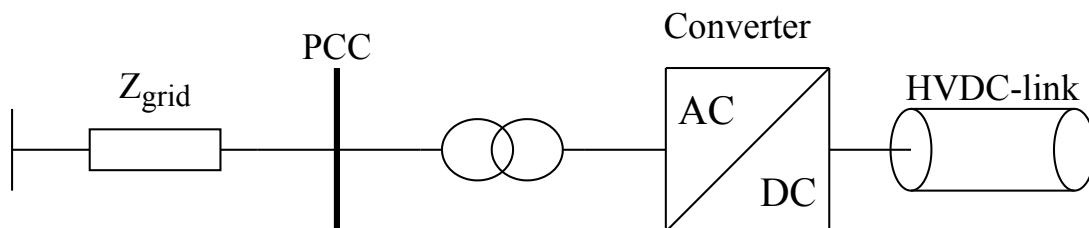


**Figure 2.5.1:** Connection of an MMC converter between an offshore AC grid and a HVDC link. The figure is from [1].

### 2.5.1 Passive & Active Impedance

Figure 2.5.2 is a representation of a MMC with its impedance contributions. The figure is from [37] and [1] and remade. The figure indicates the different contributions to the converter impedance; the passive- and active components. The passive component consists of the impedance of the transformer, the arm reactors and possible AC filter branches. The active component consists of the control system of the converter and dynamics such as filters and delays. When making a converter model, it is possible to exclude the active component of the impedance to decrease the degree of complexity. Although, this results in a less accurate model. [1, 37]

In the figure, the transfer functions of the current and voltage control loops are represented by $C_I$ and $C_V$, respectively. $V_{Synth}$ illustrates the synthesizing of the reference voltage signal and $V_{PEH}$ represents the voltage drop caused by non-ideal behavior of the power electronic hardware. [1, 37]
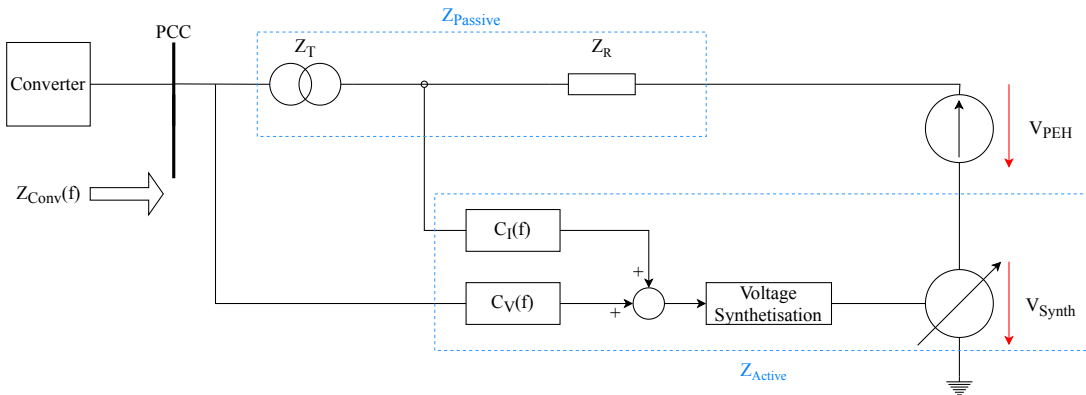


**Figure 2.5.2:** Representation of the converter and its active and passive components of impedance. This representation can be used in harmonic analysis. The figure is inspired from [37] and [1].

The difference in converter impedance when the active components are both included and omitted is presented in [1] and [37] in a Bode plot. The resulting Bode plot of the converter is presented in figure 2.5.3.
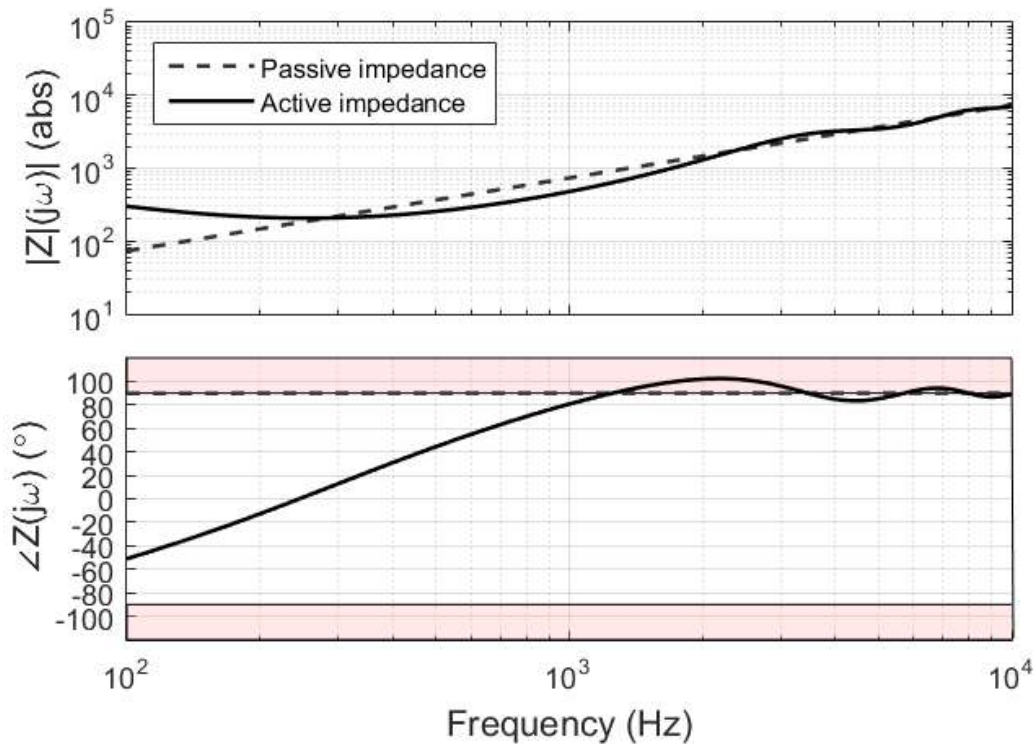


**Figure 2.5.3:** Bode plot of the passive and active impedance of the converter. The figure is from [37] and [1].

In the phase angle plot, the two red areas represent the threshold of active impedance, also called negative resistance or negative damping. This is a property in an electrical circuit where a device does not put up a potential drop in opposite direction of the incoming current, but in stead creates an electromagnetic force that boosts the current flow. This results in an injected of energy into the circuit. This phenomenon is a characteristic of so called active components.

A component is active, or exhibits negative damping, when it operates outside the phase angle specter of -90° < $\phi$ < 90°. [1, 37]

When studying figure 2.5.3, it is observed that the passive impedance phase angle is constant 90° for every frequency, while the active impedance varies with the frequency and overshoots 90° at approximately 1 kHz before it oscillates and pushes closer to the passive impedance at high frequencies. The phase angle of the active impedance introduces more damping to the system compared to the phase angle of the passive impedance between 100 Hz and 1 kHz. This is beneficial during resonance events, since the converter damps the electromagnetic natural frequencies and further mitigates the resulting network resonances. Above 1 kHz, the active impedance crosses the 90°-threshold, resulting in the converter exhibiting negative damping. This leads to negative resistive behavior at this frequency range. [1, 37]

### 2.5.2 Harmonic Resonance Analysis

Harmonic Resonance Analysis investigates the interaction between the converter- and grid impedances. In such a study, the interplay between the equivalent system resonances and the active behavior of the connected converter is of special interest. If the system exhibits a resonance frequency in the corresponding frequency range as the converter exhibits negative damping, continuous emission of the harmonic components located within this resonance will occur. Consequently, unstable operation would ensue and the protection system would trip. Such a system can be as the one illustrated in figure 2.5.1, further simplified in figure 2.5.4. The figure includes the control system, on which the converter impedance depends.
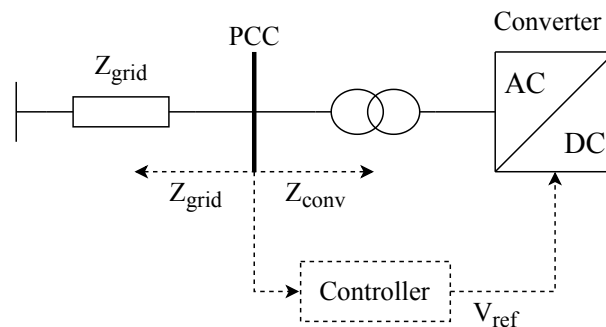


**Figure 2.5.4:** Generic example of a converter connected to a grid. The impedance of the converter depends on the controller behavior. [1, 37]

Figure 2.5.5 presents an example case from [37] where Harmonic Resonance Analysis is performed. The converter- and grid impedances are derived, and the equivalent impedance is calculated. An equivalent resonance frequency is formed when the magnitude of the converter- and grid impedances intersect. The difference in phase angles decides the damping of the resonance. The closer this difference is to 180°, the more the resonance is magnified. It is observed that the equivalent impedance has a resonance at 1 420 Hz. At this frequency, the phase difference is close to 180°. Furthermore, for frequencies where the converter is characterized as an active component, this resonance may be further worsened. In the illustrated case, this occurs between frequencies of 1 420 Hz and 3 600 Hz. [1, 37]

In [37], an Electromagnetic Transient (EMT) simulation of this system is performed. In the a simulation, the system is injected by a current at a frequency of 1 420 Hz and the voltage response at the PCC is analyzed in the time-domain.The result is a more and more increased distortion of the voltage due to the active behavior of the converter, illustrated in Figure 2.5.6. [1, 37]
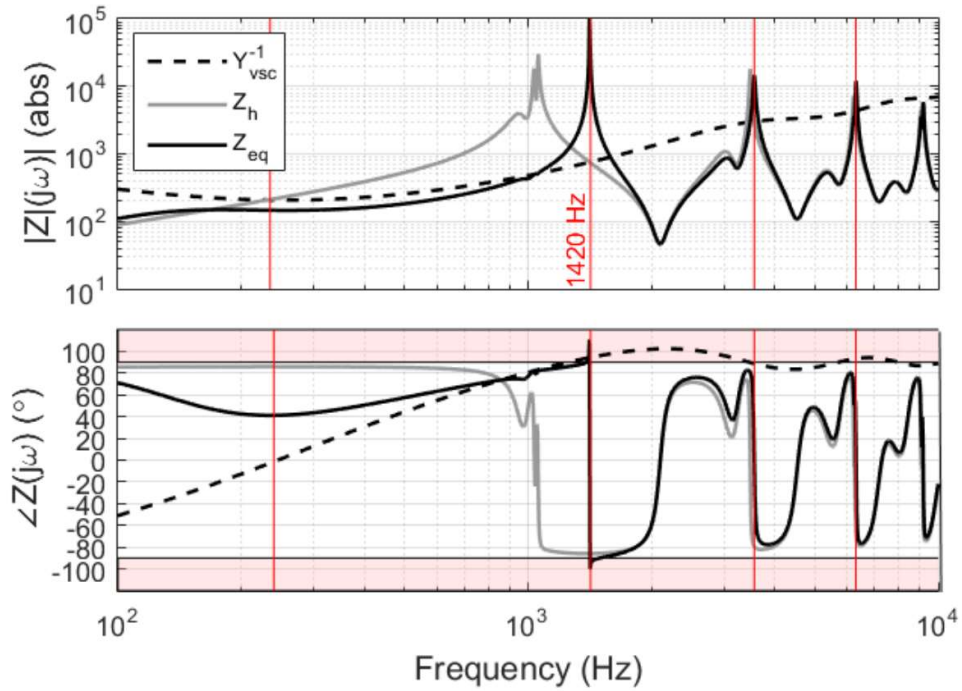
**Figure 2.5.5:** Bode plot of the converter, grid and equivalent impedances and phase angles. The figure is from [1] and [37].
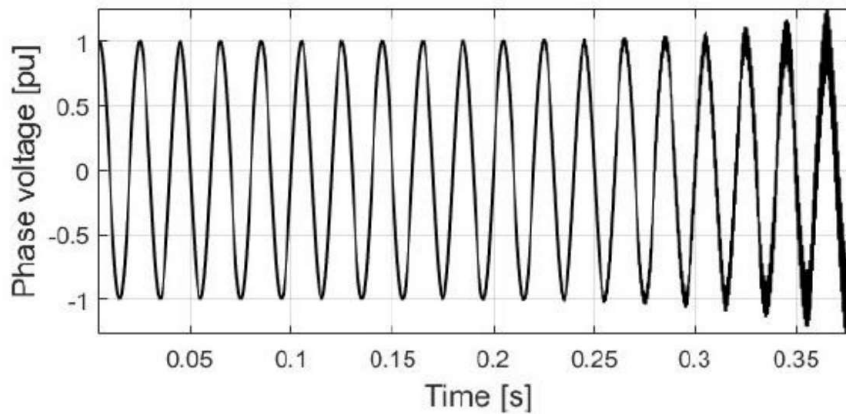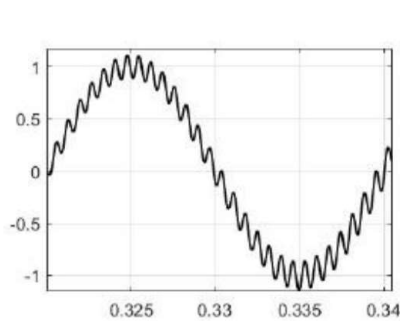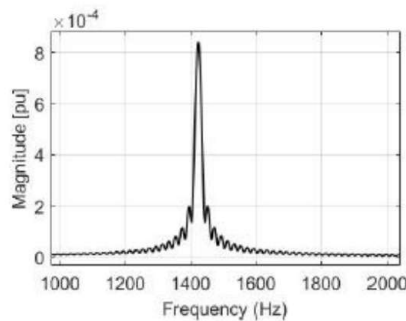


**Figure 2.5.6:** Resulting EMT time-domain simulation, illustrating a) the voltage degradation after injecting a current of 1 420 Hz, b) the phase voltage during one period, and c) the result of a FFT during the simulation time period. The figure is from [1, 37]

## 2.6    Effects of Control Parameters on Converter Impedance

The increase in power generation units that utilize power electronics also increases the need for power converter controllers. This may lead to instability issues due to the controllers ability to affect the frequency response of the converter. This was the case with an offshore wind farm in the German North Sea, showcased in [38]. The OWF was connected to the onshore grid by VSC-HVDC and experienced oscillatory voltage behavior caused by control interaction due to sensitivity to grid resonances. This example, among others, has lead to a growing interest in grid-connected converter stability analysis among stakeholders within the power system, like system operators, power electronic manufacturers and academia, although a lot of research is still needed to fully understand the relationship between controller and frequency response [38]. This section elaborates on what other research papers have found on the subject, although, to the author's knowledge, no other research has been put into the same type of system as in this thesis. Consequently, other mixtures of converter- and control schemes may not have the same behavior as the one investigated in this thesis.

### Source 1

In [39], the stability of a MMC converter connected to an AC grid was assessed by analyzing the AC-side admittance in relation to the grid impedance. This was done by making a linear analytical model of the current control schemes and the phase-locked loop, in addition to verifying the analytical model with experimental testing. The desired features of the converter admittance are low magnitude and limited phase rotation around the fundamental frequency. It was found that the converter control parameters had a strong impact on the admittance and the stability of the assessed system. In order to determine the different contributions to the AC admittance, the different control elements were added progressively, starting with the converter operating with fixed reference values. Accomplishing this revealed that:

- the AC-side current controller have a beneficial impact on the converter admittance, since it lowers the admittance magnitude without reversing the phase.

- the circulating current controller has little impact on the admittance and phase.

- removing the fixed AC-voltage reference while adding the PCC voltage feedforward greatly lowers the admittance magnitude and increases the phase rotation around the fundamental frequency.

### Source 2

In [40], the high frequency response of a HVDC-MMC station connected to an AC grid is derived using both an analytical- and an EMT model. Similarly to the previous research paper, [39], the control parameter impacts are investigated. The control structure is divided into an upper- and lower level control. The upper level includes an outer- and inner control, while the lower level controller contains the circulating current controller and regulates the submodule-capacitor voltages in each arm. The main conclusions from the research paper are:

- The impact of the lower level control is mainly restricted to the harmonic current injection and not on the impedance of the system.

- The time constant within the inner control loop determines if the impedance behaves as an equivalent inductance or capacitance. For a slow dynamic, ie. 10ms, it behaves as an inductor, while for a fast dynamic, ie. 2ms, it behaves as a capacitor.

- It s revealed that an increase in time delay increases the phase angle. High time delays may result in negative resistance behavior at high frequencies. This term is explained in

section 2.5.

## Source 3

In [41], high frequency resonance when a VSC-HVDC connects to a Doubly Fed Induction Generator (DFIG) is investigated. This is accomplished by impedance modeling the DFIG and VSC-HVDC analytically. In addition, the impact of control delay on the stability is analyzed, and counteracting measures in the form of an additional voltage controller is proposed. The report derives equation 2.6.1 for the impedance of the VSC-HVDC, $Z_{HVDC}$, in the abc frame. $H_{wv}$ and $H_{wi}$ are the voltage and the current controllers, respectively. $H_d$ is the control delay of the wind farm side of the HVDC-scheme. $Z_c$ represents the impedance of the filter connected at the wind farm side of the HVDC-scheme.

$$Z_{HVDC} = \frac{N_z(s)}{D_z(s)} = \frac{Z_c(s) + H_{wi}(s - j\omega_0)H_d(s - j\omega_0)}{1 - \big(1 - H_{wv}(s - j\omega_0)H_{wi}(s - \omega_0)\big)H_d(s - j\omega_0)} \qquad (2.6.1)$$

By analyzing the equation, it is observed that the numerator, $N_z(s)$, depends on the filter impedance and the current control delay. With an increase in frequency, the filter impedance increases while the current control delay decreases. This results in a dominance of filter impedance of $N_z(s)$ at high frequencies. Since the filter has an inductive behavior at high frequencies, as illustrated in the report, $N_z(s)$ will approach 90° at high frequencies. By plotting the transfer functions of the nominator and the denominator separately, it becomes clear that the phase angle of the denominator, $D_z(s)$, varies periodically due to the control delay and exceeds the 90°-threshold more frequently at higher frequencies. Consequently, when analyzing the bode plot for the total impedance, the resulting phase exceeds the 90°-threshold for the same frequencies as $D_z(s)$. For these frequencies, the converter can be characterized as exhibiting negative damping. The report then concludes that the periodical negative resistance behavior is introduced by the control delay and that introducing more delays increases the instability of the system.[41]

## Source 4

The relationship between the time delay and stability of a single-loop controlled grid-connected inverter employing inverter current feedback or grid current feedback is investigated by [42]. It is found that the existence of time delay weakens the stability of the inverter inhabiting the respective control scheme. An important observation made in the report is that larger time delays results in a crossing the -90° threshold at lower frequencies. [42]

# Chapter 3

# Offshore Wind Farm Model

A model of an offshore wind farm is needed to achieve the goal of this thesis. Since offshore grids are dominated by subsea cables, PSCAD is the chosen software because of its highly detailed cable models. Due to time constraints, the model part of this project is based on pre-existing models in PSCAD's knowledge base. Adjustments have been made where necessary. The predominant source of the model is [43]. This chapter provides insight into the most relevant parts of the model that lays the foundation for further Harmonic Resonance Analysis. Consequently, modeling of the mechanical components such as the PMSG and its control scheme is omitted.

## 3.1 Overview of system

Figure 3.1.1 presents the topology of the OWF model. The terms "generator-side" and "grid-side" use the fully rated converter as reference to specify the location at question. The model consists of:

- A Type-IV wind turbine, consisting of a permanent magnet synchronous generator and a fully rated converter utilizing 2-level voltage source converters.

- Two LCL-filters; one on the-generator side and one on the grid side.

- A minimum of 3 transformers. The number is determined by the number of strings defined by the scaling unit. For each string added, a new equivalent transformer is also added.

- 3 coaxial cables connecting a turbine string to another, creating a collection circuit.

- A scaling unit used to make a representation of an aggregated wind farm. The current from one string is simply multiplied with the defined number of strings to get the aggregated model.

- A HVAC transmission grid. Modeled as a tower-transmission scheme.

- A representation of the onshore grid.
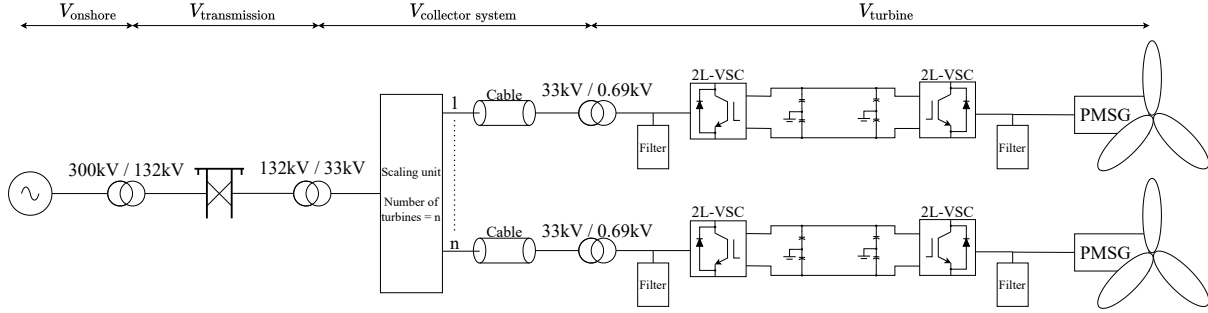
**Figure 3.1.1:** Topology of OWF model.

## 3.2 AC-DC-AC Converter

The AC-DC-AC converter implemented is a fully-rated converter consisting of two back-to-back Voltage Source Converters, which are modeled as switching models. The design of the switching model is described in Section 3.2.1. The grid-side converter controls the DC-link voltage, covered in Section 3.2.2, while the generator-side converter controls active power flow from the turbine, described in Section 3.2.3. A capacitor is installed to reduce the DC-voltage ripple in the DC-link. The design of this DC-capacitor is explained in Section 3.2.4. The design parameters are summarized in table 3.2.1.

**Table 3.2.1:** Summary of converter design parameters.

| Parameter | Symbol | Value |
|---|---|---|
| Switching frequency | $f_{sw}$ | $2\,500\,\mathrm{Hz}$ |
| Converter inductance | $L_{inv}$ | $0.3063\,\mathrm{mH}$ |
| DC-link capacitor | $C_{DC}$ | $15\,000\,\mu\mathrm{F}$ |

### 3.2.1 PWM Switching Scheme and Design of Converter Inductance

The switching model in this thesis is a Pulse-Width-Modulated switching scheme. The principle of switching is the same for both the grid- and generator side converter, but the switching pulses are determined differently for the two. In short, the switching logic is identical for the two, but different factors trigger the switching in the respective converters. Figure 3.2.1 illustrates the full-bridge converter schematic. The converters are installed with IGBTs in order to implement PWM.
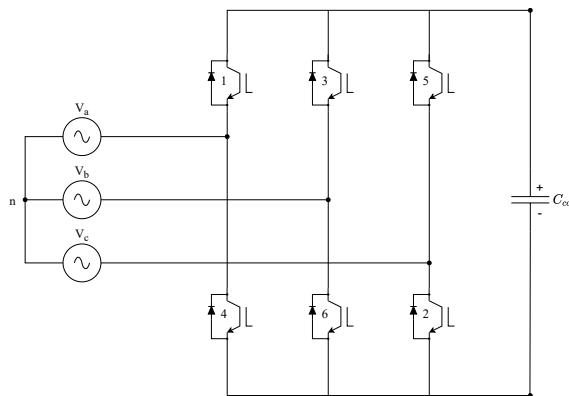


**Figure 3.2.1:** Full-bridge schematic of 2L-VSC.

The IGBTs are activated by a pulse generated by a switching logic. This switching logic is based on comparing reference voltage values and a triangular carrier signal. The reference voltage values is generated, in per unit, by the respective controller of the converters, while the triangular signal is generated by the *Sawtooth Generator*-block in PSCAD where maximum- and minimum output levels are defined as ± 1, which makes comparing it to the reference voltage possible. Figure 3.2.2 shows how the pulses to IGBTs 1 and 4 are generated. The pulses to the other four IGBTs are excluded from the figure to simplify the illustration. When $V_{Ref} >$ Carrier, Pulse 1 is sent to IGBT 1, making it conduct. At this time, IGBT 4 if off. When $V_{Ref} <$ Carrier, Pulse 4 is sent to IGBT 4, making it conduct. At this time, IGBT 1 is off. The signals for the other IGBTs are generated following the same logic.
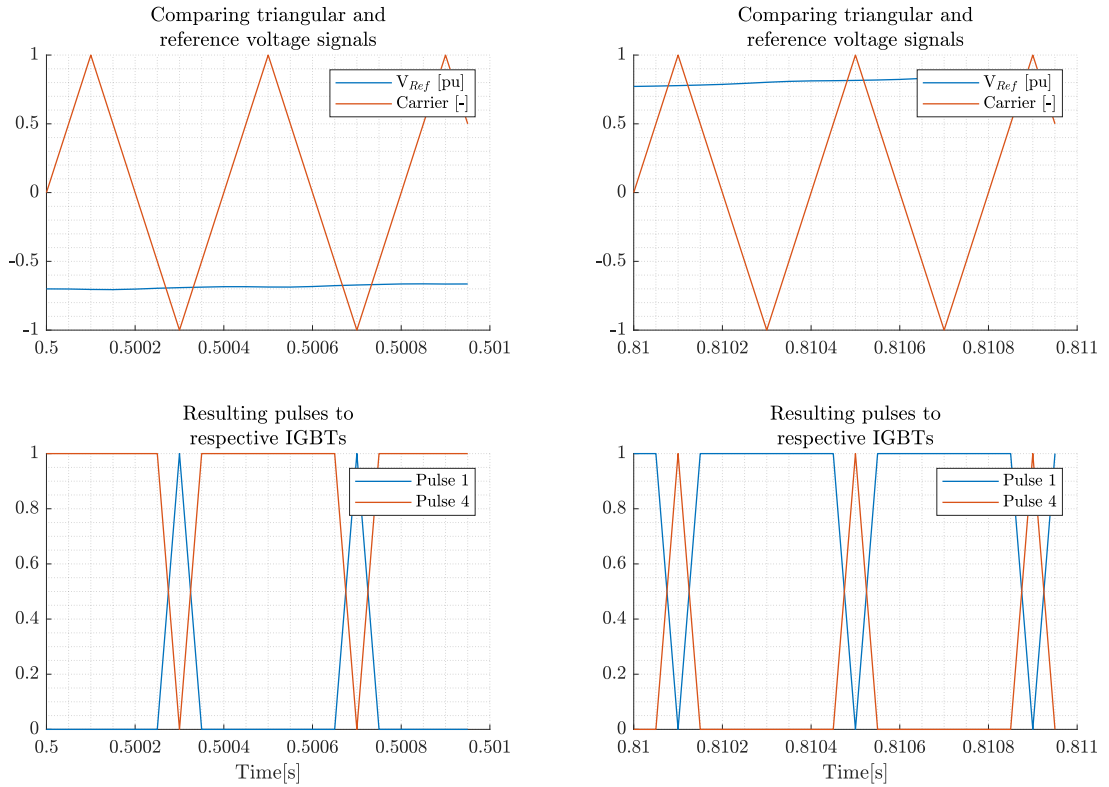


**Figure 3.2.2:** Illustration of how pulses to IGBTs in a switching scheme functions.

Another important parameter of the carrier signal is its frequency, $f_{\text{carrier}}$. This frequency also establishes the switching frequency of the converter. An increase in switching frequency also increases the total losses due to switching losses, but it also reduces the amount of harmonic emission [44]. Switching frequencies for VSCs are usually between 1-2 kHz, but because a low THD of the output signals from the converter is of great importance, a switching frequency of 2.5 kHz is chosen [45]. According to [46], equation 3.2.1 can be used to calculate the converter inductance based on the DC-link voltage, $V_{\text{DC}}$, switching frequency, $f_{\text{sw}}$, and peak-to-peak amplitude of the ripple current, $I_{\text{rpp}}$, which is assumed to be 20% of the peak-to-peak nominal current.

$$L_{\text{inv}} = \frac{V_{\text{DC}}}{4 \cdot f_{\text{sw}} \cdot I_{\text{rpp}}} \tag{3.2.1}$$

The nominal current, $I_{\text{nom}}$, can be calculated by applying equation 3.2.2. This can further be used to calculate the peak-to-peak nominal current by implementing equation 3.2.3.

$$I_{\text{nom}} = \frac{P_{\text{conv}}}{\sqrt{3} \cdot V_{\text{L-L rms}}} \tag{3.2.2}$$

$$I_{\text{nom,peak-to-peak}} = \sqrt{2} \cdot I_{\text{nom}} \tag{3.2.3}$$

The peak-to-peak amplitude of the ripple current is then calculated by applying equation 3.2.4.

$$I_{\text{ripple}} = 0.2 \cdot I_{\text{nom,peak-to-peak}} \tag{3.2.4}$$

By implementing the values provided in table 3.2.2 together with the predefined equations, the converter inductance becomes:

$$L_{\text{inv}} = \frac{1.45\,\text{kV}}{4 \cdot 2.5\,\text{kHz} \cdot \frac{2.0\,\text{MW}}{\sqrt{3} \cdot 0.69\,\text{kV}} \cdot \sqrt{2} \cdot 0.2} = 0.0003063\,\text{H}$$

**Table 3.2.2:** Overview of values used for converter inductance calculation.

| Parameter | Value |
|---|---|
| $V_{\text{DC}}$ | 1.45 kV |
| $f_{\text{sw}}$ | 2.5 kHz |
| $P_{\text{conv}}$ | 2 MW |
| $V_{\text{L-L rms}}$ | 0.69 kV |

In order to perform Harmonic Resonance Analysis with sufficient accuracy, the current- and voltage signals prior to the analysis has to contain a low amount of harmonics. The designed inductor is a high-impedance component for high frequencies, which means that the amplitude of harmonic current components of high orders is reduced.

Figure 3.2.3 depicts part of the current- and voltage signals from the grid side of the converter. In addition, the figure shows the harmonic components revealed by Fast-Fourier Transform. No filter is implemented at this stage. A clear distinction between the current- and voltage signals is observed. The distortion of the voltage signal is much greater than the current signal. To get a measure of the distortion of the signals, the total harmonic distortion is calculated. For the readers convenience, equations 2.2.2 and 2.2.3 for the total harmonic distortion of current and voltage signals, respectively, are repeated in equation 3.2.5 and 3.2.6. The calculation is performed in MATLAB and the results are listed in table 3.2.3. According to [47], the voltage distortion limits are dependent on the system voltage. For systems with a voltage below, or equal to, 69 kV, the total voltage distortion limit is 5.0 %. The current distortion limits are dependent on the ratio between the maximum short circuit current at the location in question and the maximum demand load current over a certain timeframe. This ratio is not calculated in this thesis, but the lowest limit for harmonic current distortion listed in [47] is 5.0 %. The distortion of the voltage signal is much greater than the allowed limit while the current signal is well below the respective limit. Based on this information it becomes clear that a filter is needed in order to be able to perform Harmonic Resonance Analysis.
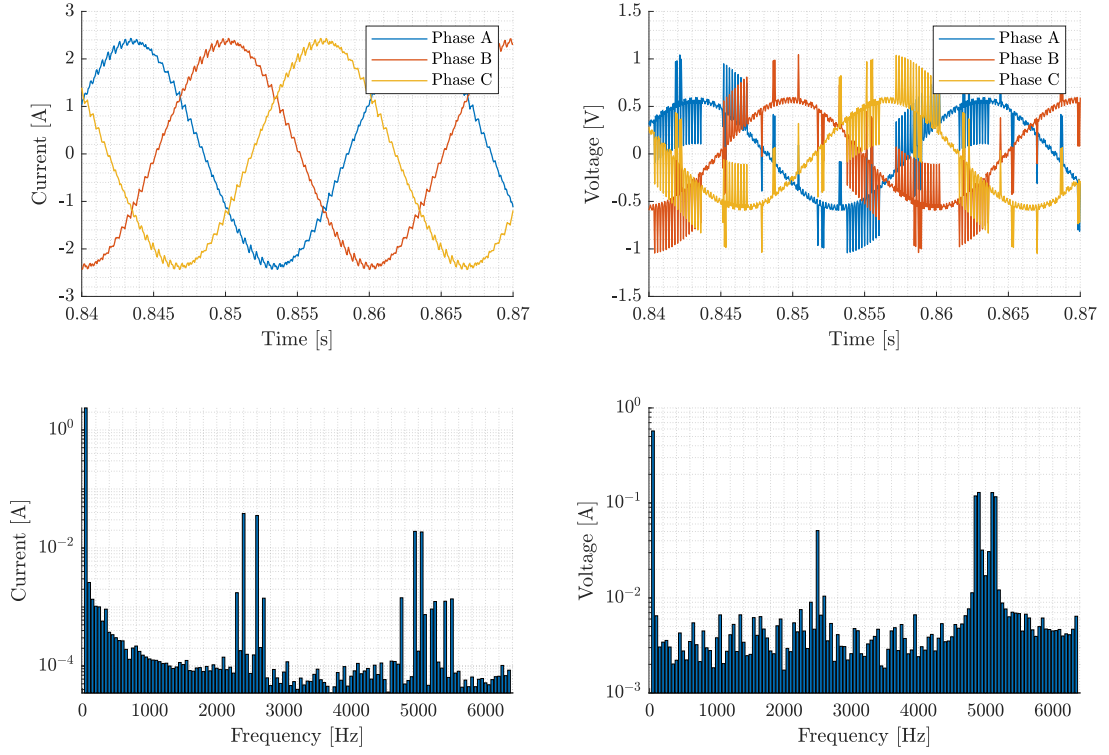
**Figure 3.2.3:** The figure depicts part of the current- and voltage signals from the grid side of the converter, as well as the Fast Fourier Transform results of the respective signals. No filter is implemented. Notice the logarithmic scale on the y-axis.

$$\text{THD}_I = \frac{\sqrt{\sum_{h=2}^{\infty} I_h^2}}{I_1} \tag{3.2.5}$$

$$\text{THD}_V = \frac{\sqrt{\sum_{h=2}^{\infty} V_h^2}}{V_1} \tag{3.2.6}$$

**Table 3.2.3:** THD calculation results of current- and voltage signals on the grid side of the converter with no filter connected.

| | |
|---|---|
| **THD**$_I$ | 0.1470 % |
| **THD**$_V$ | 11.9310 % |

### 3.2.2 Grid-side Controller

Figure 3.2.4 is an illustration of the grid-side controller. The grid side controller, designed by [43], regulates the DC-link voltage and AC voltage. The DC-link voltage controller is highlighted in green and the cascaded AC voltage and reactive power controller is highlighted in blue. These controllers generate the d- and q-axis current orders, which are used further in the current controller, highlighted in red. Within the current controller, the phase voltage- and current signals undergo direct-quadrature-zero (DQ0) transformation by using the grid-side phase voltage to obtain the conversion angle used in the PLL. This makes the inverter a grid following converter. The decoupled current controller generates the reference voltage signals in q- and d-axis values before they are transformed back to three-phase reference waveforms. These are then used as input in the PWM scheme in the grid-side converter. The control parameters for the four PI-regulators and the PLL are provided in table 3.2.4. [43]

**Table 3.2.4:** Parameters used in the PI-regulators and the PLL in the grid-side controller.

| Parameter | $PI_1$ | $PI_2$ | $PI_3$ | $PI_4$ | $PI_5$ | Parameter | PLL |
|---|---|---|---|---|---|---|---|
| $K_p$ | 0.75 | 1.00 | 0.50 | 1.00 | 0.50 | $K_p$ | 50 |
| $T_i$ | 0.1 | 0.20 | 0.05 | 0.02 | 0.05 | $K_i$ | 100 |
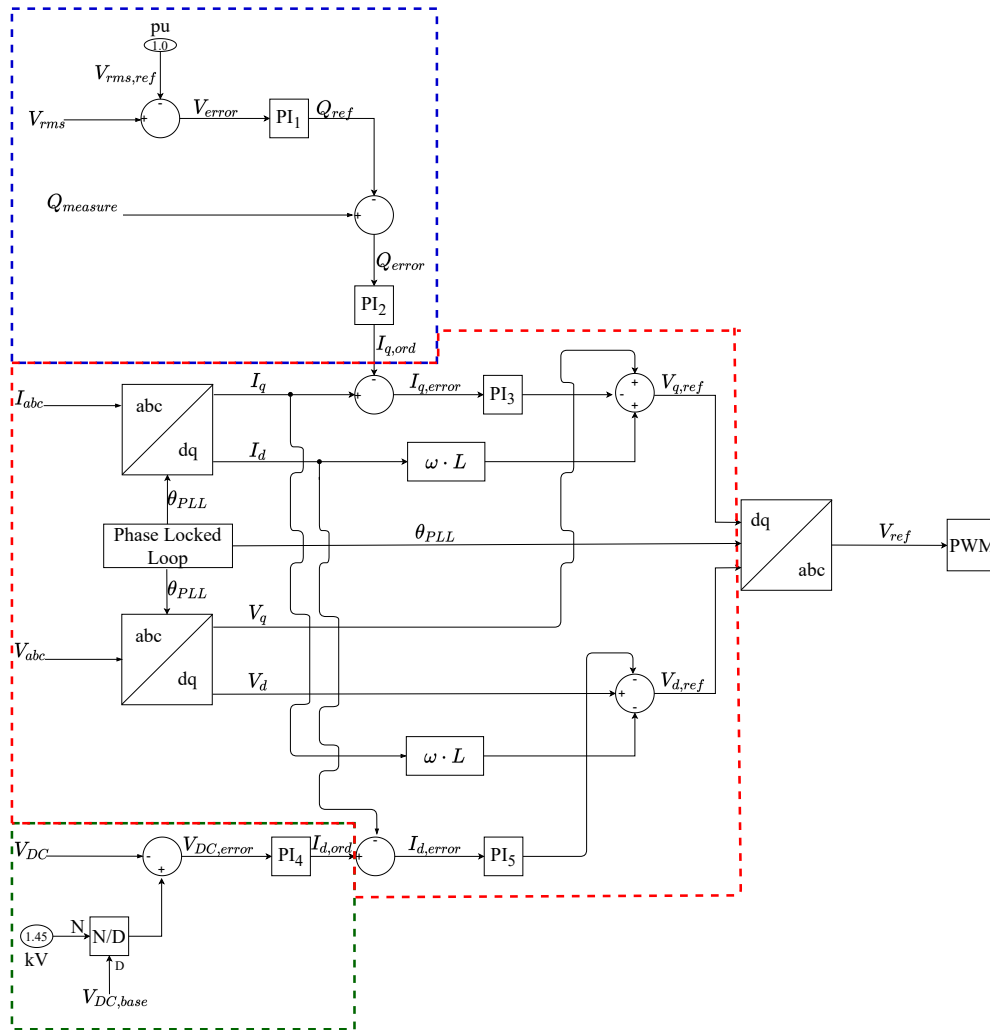


**Figure 3.2.4:** Topology of the grid-side controller. The DC-link voltage controller is highlighted in green and the cascaded AC voltage and reactive power controller is highlighted in blue. The decoupled current controller is highlighted in red.

### 3.2.3    Generator-side Controller

Figure 3.2.5 is an illustration of the generator-side controller. The controller regulates the AC voltage and active power generated in the PMSG. The active power controller is highlighted in green, where the active power transferred through the converter, $P_{\mathrm{conv}}$, is compared to the reference value of active power, $P_{\mathrm{ref}}$, obtained from the PMSG controller. The error in active power is used to obtain the d-axis current order, $I_{\mathrm{d,ord}}$, used in the current controller. The AC voltage controller, highlighted in blue, compares the measured rms AC voltage in per unit to a fixed reference value of 1 pu. The error in voltage is used to obtain the q-axis current order, $I_{\mathrm{q,ord}}$, which is further used in the current controller. Lastly, the current controller, highlighted in red, is used to obtain the reference three-phase voltage waveforms. These are used as input in the PWM scheme in the two-level voltage source converter on the generator side. [43]

**Table 3.2.5:** Parameters used in the PI-regulators and the PLL in the generator-side controller.

| Parameter | PI$_1$ | PI$_2$ | PI$_3$ | PI$_4$ | Parameter | PLL |
|---|---|---|---|---|---|---|
| $\mathbf{K_p}$ | 1.00 | 1.00 | 0.25 | 1.00 | $\mathbf{K_p}$ | 50 |
| $\mathbf{T_i}$ | 0.20 | 0.01 | 0.025 | 0.02 | $\mathbf{K_i}$ | 500 |
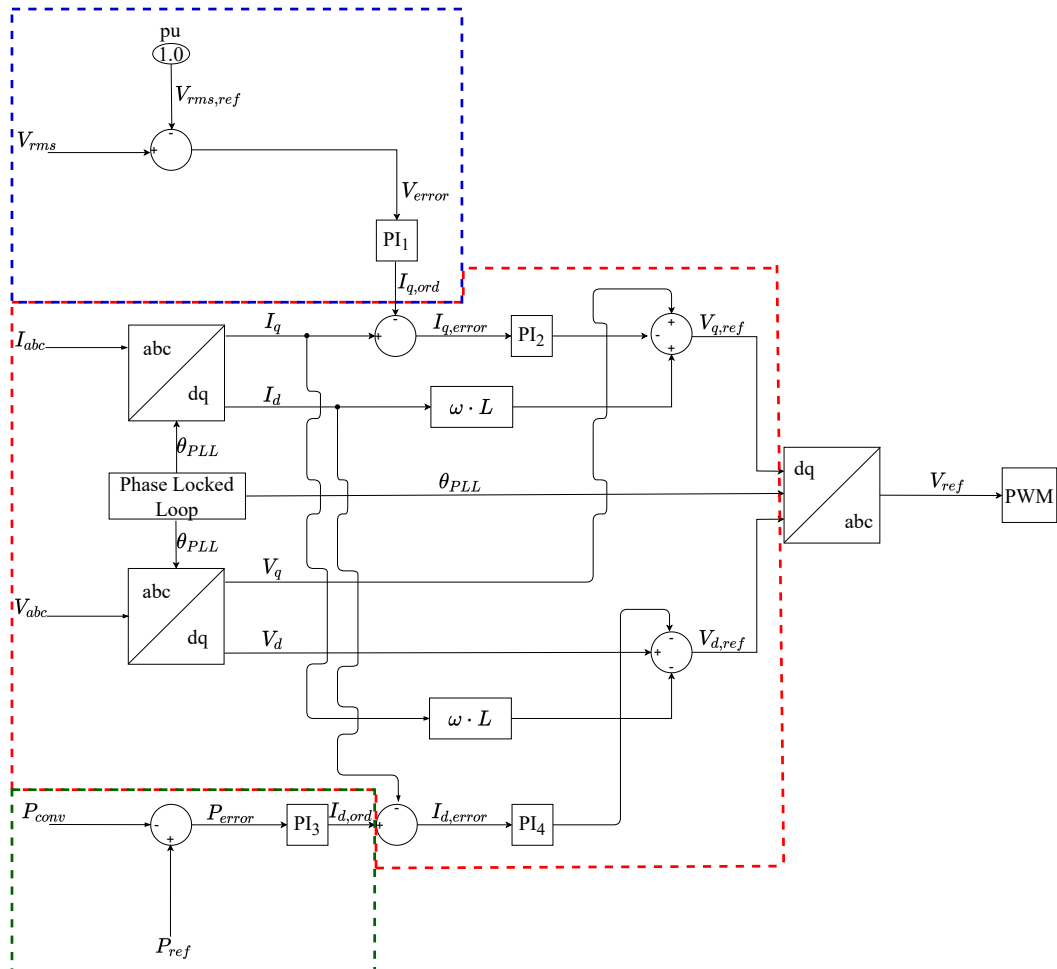


**Figure 3.2.5:** Topology of the generator-side controller. The active power controller is highlighted in green and the AC voltage controller is highlighted in blue. The decoupled current controller is highlighted in red.

### 3.2.4 DC-link Capacitor

The purpose of the DC-link capacitor is to stiffen the DC voltage and create a low-impedance path for high-frequency currents. The design of the capacitor is dependent on the modulation index, $m_a$, the angular switching frequency, $\omega_{sw}$, the allowed voltage ripple, $\Delta V_{DC}$ and the rated current, $I_r$. The modulation index is the ratio between the peak fundamental frequency output voltage and the supplied DC voltage, shown in equation 3.2.7. With the amplitude of the output voltage equal to $0.69\,\text{kV} \cdot \sqrt{2}$ and the DC voltage equal to $1.45\,\text{kV}$, the modulation index becomes 0.678. For modulation indexes in the range of $m_a <1$, the pulse-width modulation moves the harmonics up closer to the switching frequency. The drawback of such a modulation index is the lower amplitude of the fundamental frequency voltage than may be wished. Equation 3.2.8 presents how the DC-link capacitance is calculated in this thesis. With the current being $2\,\text{kA}$ and an allowed voltage ripple of 2%, the DC-link capacitance becomes $14\,883\mu\text{F}$. [46, 48, 49]

$$m_a = \frac{\hat{V}_{o1}}{V_{s,d}} = \frac{0.69\,\text{kV} \cdot \sqrt{2}}{1.45\,\text{kV}} = 0.678 \tag{3.2.7}$$

$$C_{\text{DC}} = \frac{m_a}{2\omega_{sw}\Delta V_{DC}}I_r = \frac{0.678}{2 \cdot (2\pi 2500\,\text{Hz}) \cdot (1.45\text{kV} \cdot 0.02)} \cdot 2\,\text{kA} = 14\,883\,\mu\text{F} \tag{3.2.8}$$

## 3.3 LCL filter

Figure 3.3.1 presents the topology of the LCL filter implemented in this thesis. The topology is identical to the illustration previously presented in figure 2.3.3. The reader is referred to section 2.3 for theory related to LCL filters.
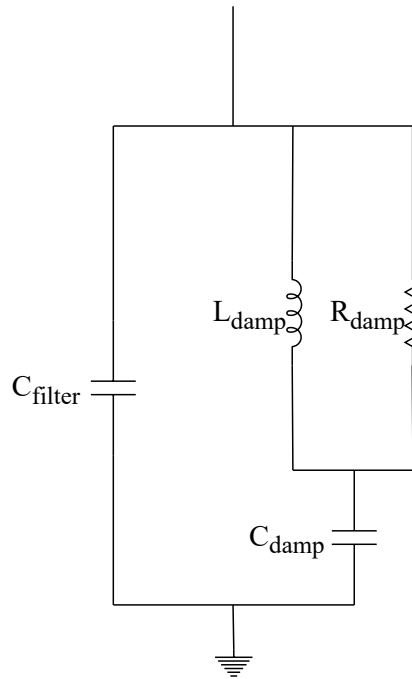


**Figure 3.3.1:** Equivalent circuit of a LCL filter.

The design process of the filter starts with the choice of cutoff frequency, $f_{\text{cutoff}}$, or corner frequency. For a low-pass filter, the cutoff frequency determines the frequency at which the frequency response of the filter starts showing negative gain. In other words, the frequency response for the filter starts having capacitive characteristics at $f_{\text{cutoff}}$. The harmonic components

start flowing through the filter at this frequency. This means that the choice of cutoff frequency is heavily dependent on the respective system.

The filter utilized in this thesis is designed by PSCAD, [43], with a cutoff frequency defined as 900 Hz. The design procedure initializes with calculating the filter capacitance, $C_{\text{filter}}$, based on the cutoff frequency and inverter inductance, $L_{\text{inv}}$, in equation 3.3.1.

$$C_{\text{filter}} = \frac{1}{(2\pi \cdot f_{\text{cutoff}})^2 \cdot L_{\text{inv}}} \tag{3.3.1}$$

The damping inductance, $L_{\text{damp}}$, is calculated by equation 3.3.2.

$$L_{\text{damp}} = 5 \cdot L_{\text{inv}} \tag{3.3.2}$$

The damping capacitance, $C_{\text{damp}}$, can further be calculated by equation 3.3.3.

$$C_{\text{damp}} = \frac{C_{\text{filter}}}{2} \tag{3.3.3}$$

Then, the damping resistance, $R_{\text{damp}}$, can be calculated with equation 3.3.4.

$$R_{\text{damp}} = \sqrt{\frac{L_{\text{damp}}}{C_{\text{damp}}}} \tag{3.3.4}$$

The resulting filter parameters are presented in table 3.3.1.

Table 3.3.1: Calculated filter parameters for the LCL filter with 900 Hz as the cutoff frequency.

| Component | Value |
|---|---|
| $C_{\text{filter}}$ | 102 $\mu$F |
| $L_{\text{damp}}$ | 1.531 mH |
| $C_{\text{damp}}$ | 51.042 $\mu$F |
| $R_{\text{damp}}$ | 5.48 $\Omega$ |

Figure 3.3.2 illustrates the current- and voltage signals measured at the grid side of the converter with the filter installed. It also presents the FFT-results of the signals. It is observed that the largest harmonics are at 2 400 Hz, 2 600 Hz, 4 950 Hz and 5 050 Hz, although their magnitudes are not high. To get a measure of the distortion of the signals, the Total Harmonic Distortion is calculated by applying equations 3.2.5 and 3.2.6. The results are listed in table 3.3.2 and it is confirmed that the installation of a filter resulted in values well below the limits defined in the IEEE-519 standard [47].

Table 3.3.2: THD calculation results of current- and voltage signals on the grid side of the converter with filter connected.

| | |
|---|---|
| $\mathbf{THD}_I$ | 0.3085 % |
| $\mathbf{THD}_V$ | 0.1647 % |
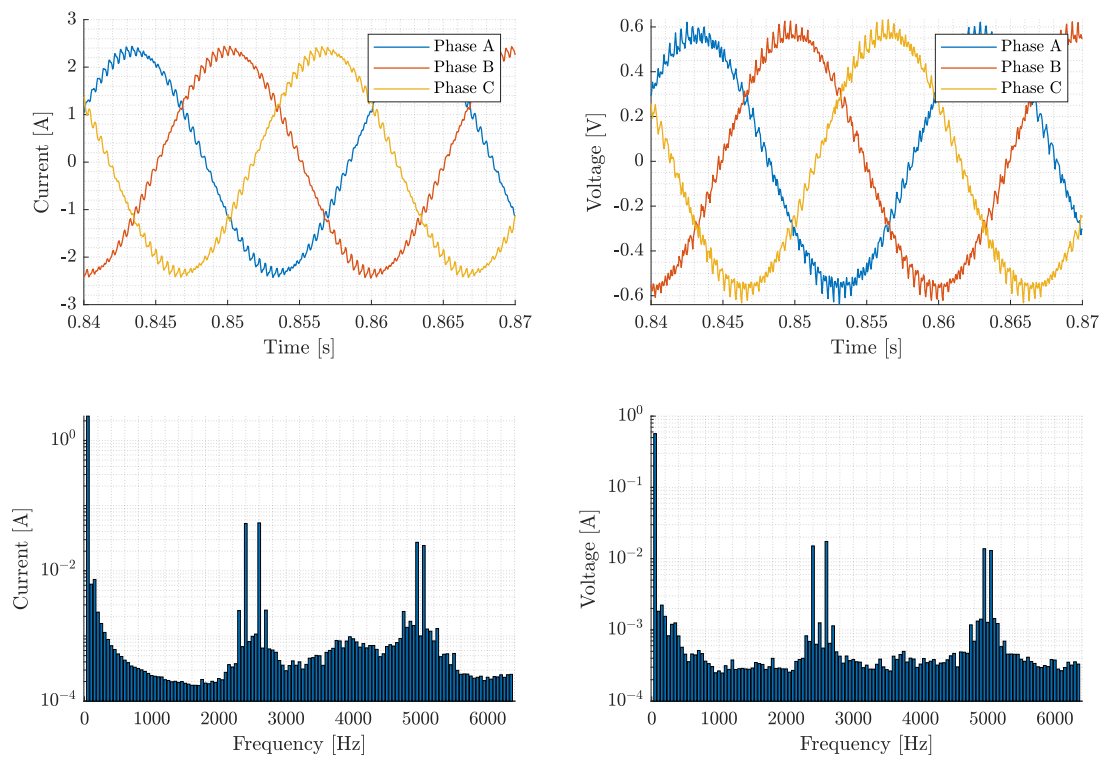
**Figure 3.3.2:** The figure depicts part of the current- and voltage signals from the grid side of the converter, after the filter is connected,as well as the Fast Fourier Transform results of the respective signals. Notice the logarithmic scale on the y-axis.

## 3.4   The offshore collector system

An offshore collector system consists of underwater cables that connect the wind turbines within the wind farm. This interarray system enables the generated power by each unit to be exported to the respective substations. Due to the wake effect, turbines have to be spaced by a certain number of rotor diameters. This causes long cabling distances, which increases the losses in the system. These losses are regarded as the largest source of losses in offshore wind farms. Normally, it would be of import to minimize these losses, but this is not of consideration in this thesis. The distance of each string is decided to be 5 km from turbine to substation. This distance is made up of three cables carrying each phase. Figure 3.4.1 illustrates the cable cross-section with dimensions implemented in this thesis. [4]

The cable is a default simplified model designed by PSCAD and is based on typical values for material data. It is modeled as a frequency dependent component, also called a universal line model. This makes it possible to measure the frequency dependency of all line parameters, which is necessary during studies where harmonic behavior is important. The defined cable parameters is presented in table 3.4.1.
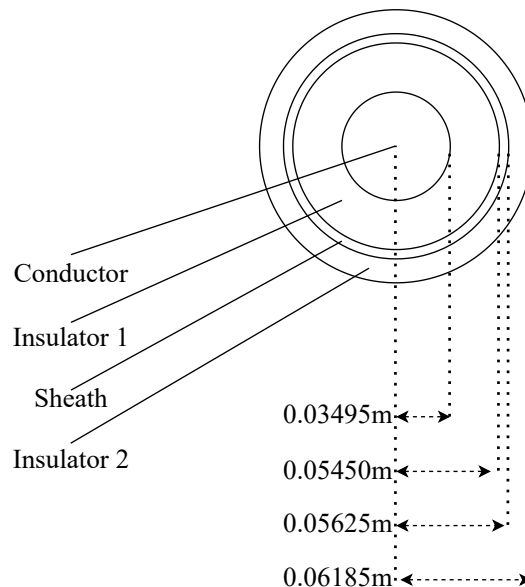


**Figure 3.4.1:** Cable cross-section, including dimensions of the conductor, insulators and sheath, used in the offshore collector system.

**Table 3.4.1:** Cable parameters used in the interarray system.

| Conductor | |
|---|---|
| DC resistance | 0.01288 Ω/km |
| Resistivity | 1.68e-8 Ω·m |
| **1st Insulating Layer** | |
| Capacitance | 0.20599 $\mu$F/km |
| Relative permittivity | 2.3 |
| **Sheath** | |
| DC resistance | 0.101 Ω/km |
| Resistivity [ohm*m] | 1.68e-8 Ω·m |
| **2nd Insulating Layer** | |
| Property given as | Relative permittivity of polyethylene |
| Capacitance | 0.20599 $\mu$F/km |
| Resisitivity | 2.3 |

# Chapter 4

# Methods for System Impedance Derivation

An important characteristic of impedance-based analysis is to be able to obtain the impedance equivalent of a system from simulations and measurements. There are many methods that can be applied to achieve this, with varying degree of accuracy. A crucial factor that decides what method to implement is the available information about the system. Often in systems containing power electronic converters, the information regarding the converter's control parameters is not available.

This chapter introduces different methods for obtaining the system impedance. Section 4.1 provides an overview of techniques that either fails to include dynamic behavior or demands full insight into the working parameters of the given system. Section 4.2 dives into a technique used to derive the system impedance of systems where the converter can be "black boxed".

## 4.1 Summary of Different Resonance Analysis Techniques

There are different methods that can be applied in harmonic resonance analysis and all techniques have their pros and cons. In [1], all of the following techniques are elaborated on and reviewed in more depth. This section provides the reader with a short summary of the investigated techniques that either fail to include dynamic behavior of the system or demands full knowledge of all system parameters to be implementable.

### 4.1.1 Frequency Scan of Stationary System

Frequency scan of a stationary system is the simplest resonance analysis technique to implement. The definition of stationary is the assumption that all power electronic components are in their off state. The method calculates the frequency response of a network at a given bus in the network. This is done by, first, injecting a 1 per unit sinusoidal current into a bus. Then, the voltage response is measured. The injected current and the measured voltage at bus $i$ corresponds to the driving point impedance at frequency $f$. This is illustrated by Equation 4.1.1. [1, 50]

$$Z_{ii}(f) = \frac{V_i(f)}{I_i(f)} \qquad (4.1.1)$$

This calculation is iterated for fixed frequency steps of $h \cdot f_f$ up to a predefined limit. $Z_{ii}$ is the driving point impedance, $V_i$ is the measured voltage at bus $i$ and $I_i$ is the injected current at bus $i$. By plotting the impedance frequency response, possible harmonic resonance conditions for a stationary system is detected [1, 50].

Although the technique clearly indicates the resonance frequency of the stationary system, it does not provide information on what component is responsible for the resonance or where to most efficiently mitigate the problem [1, 51]. Another challenge related to frequency scans of stationary systems is considering different operational scenarios. This is especially true for wind farms. The actual impedance of the system is dependent on the number of turbines in operation, the switching of the capacitor banks at substations, the controller of the converters and the impedance of the grid as a function of the frequency, or grid harmonic impedance [1, 25]. In short, the technique does not allow analysis where the effect of controllers are accounted for.

### 4.1.2   State-Space Modal Analysis

Another technique applied to identify possible instabilities of a power system is State-Space Modal Analysis (SSMA). This entails performing an eigenvalue analysis of the produced state-space representation of the power system [1, 52]. By finding the eigenvalues of the state matrix, called the eigen-modes of the system, the harmonic resonance frequency is revealed. In addition, eigenvalue analysis provides better information on the participation of each bus in the network [1, 52].

State-Space Modal Analysis can be a powerful tool. It has the potential to reveal possible unstable modes and what factors contribute the most to the instability in addition to including the dynamic behavior of the system, e.g active impedance of converters. Although, representing the dynamic behavior, including the frequency dependency of all components in a wide range of frequencies, of the electrical system in State-Space may be a considerable challenge. In addition, to include converters in this representation demands detailed information about the controller data, which is not always possible. [1, 37]

### 4.1.3   Harmonic Resonance Mode Analysis

Harmonic Resonance Mode Analysis (HRMA) is based on eigenvalue-decomposing the admittance- or impedance matrix at different frequencies, identifying the critical mode and the corresponding critical eigenvectors. This information can be used to determine the resonance frequencies of the system and the participation factors of the respective components subject to this analysis. This enables identification of the most efficient location to apply mitigating measures regarding resonances. [1, 53].

Similarly to State-Space Modal Analysis, it is possible to include impedance models of converters in HRMA, but it demands full knowledge of the working parameters of the converters in the system. In contrast, it may be more easily implementable technique to study harmonic resonance than SSMA is. [1, 54]

## 4.2 Current/Voltage Perturbation Technique

It is possible to derive the frequency response of a system by performing measurements on the terminals of the system. When doing this, the system has to be perturbed by either a voltage- or current injection. Then, the response of the system is measured and the impedance model is calculated. This technique is called the Current/Voltage Perturbation Technique.

Before performing the Current/Voltage Perturbation Technique, there are important considerations that have to be made. Figure 4.2.1 illustrates two approaches to the Voltage/Current Perturbation Technique. The two approaches are, as the name suggests, whether the system is perturbed by a series voltage or shunt current injection. The system can be divided into two subsystems; the source (converter) and the load (grid).
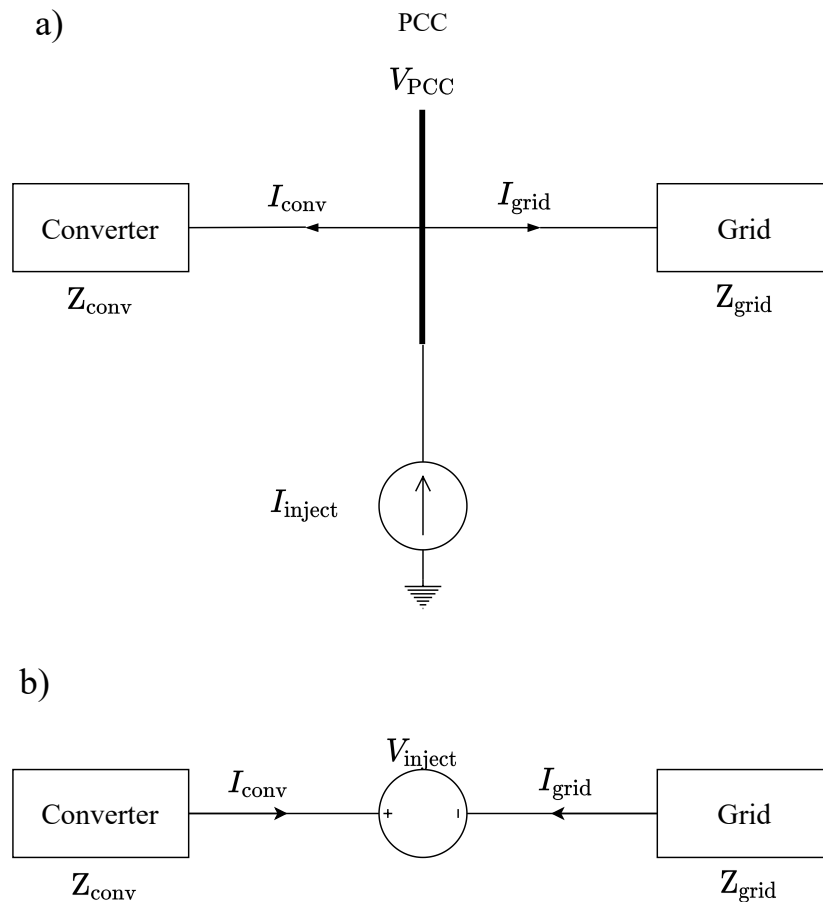
**Figure 4.2.1:** Illustration of two approaches to the Voltage/Current Perturbation technique: a) shunt current injection and b) series voltage injection.

According to [55], for numerical simulations, the chosen method has little impact on the results. For experimental setups, however, the injection types provides accurate results for different subsystems. The shunt current injection gives higher accuracy than the series voltage in low-impedance systems, and vice versa. This thesis focuses on simulations, so experimental considerations are not given further notice. The chosen injection type for this thesis is the shunt current injection. After the injection method is selected, the frequency step and range for the injections is selected. It is important to omit the fundamental frequency from the frequency range because the presence of the background voltages and currents corrupt the impedance calculation at the fundamental frequency [56]. The range should also be chosen with the system in mind. In this thesis, the system is an offshore grid, meaning a high frequency range is relevant,

and the IEC standard states that the highest allowed harmonic order is the 99th. This means with a fundamental frequency of $50\,\text{Hz}$, analysis above $4\,950\,\text{Hz}$ is meaningless [48]. For this thesis, however, the chosen frequency range is from $100\,\text{Hz}$ up to $5\,100\,\text{Hz}$. The reason for the higher upper limit than the standard is because of practical matters in PSCAD.

The next consideration is the amplitude of the injected harmonic currents. The individual impedances of the grid and converter can be very different, so to get the correct frequency response of the respective subsystems may demand several trial and error simulations where the amplitude is altered. Although, it is recommended that the amplitude of the injected current not exceeds 1%-10% of the RMS current at the point of injection. If the converter is modeled as a switching model, this step may be very time consuming. The component named *Harmonic Current Injection* can be found in the PSCAD library and is used to inject the model with an array of harmonic currents with specified amplitudes and within a given frequency range.[55, 56]

Once the system is perturbed, the voltage at the point of connection ($V_{\text{PCC}}$), converter current ($I_{\text{conv}}$) and grid current ($I_{\text{grid}}$) needs to be stored. This is in order to perform Fast Fourier Transform to get the frequency components within the signals. In this thesis, PSCAD is used to perform the transform. The component applied, named *On-Line Frequency Scanner*, is shown in figure 4.2.2. The component determines the harmonic magnitude and phase of the input signal as a function of time, up to a certain amount of harmonics [57]. The user inputs the base frequency and the number of harmonics, e.g. the user can choose a base of $50\,\text{Hz}$ and 255 harmonics, resulting in a FFT going up to $12\,750\,\text{Hz}$. For this thesis, to be able to capture potential resonance frequencies, a smaller frequency increment is of interest. To be able to do analysis of up to the IEC standard at the same time as a sufficient resolution is upheld, the analysis is divided in three intervals. The first is with a base of $10\,\text{Hz}$, resulting in a range between $100\,\text{Hz}$ and $2\,550\,\text{Hz}$. The second is with a base of $15\,\text{Hz}$, resulting in a range between $2\,600\text{Hz}$ and $3\,825\,\text{Hz}$. The third is with a base of $20\,\text{Hz}$, resulting in a range between $3\,840\,\text{Hz}$ and $5\,100\,\text{Hz}$. The component can also be used to calculate the symmetrical components of each harmonic.
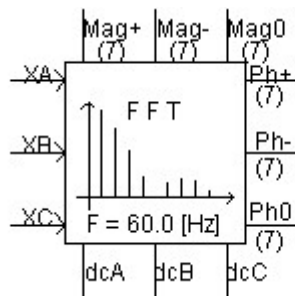


**Figure 4.2.2:** On-line frequency scanner in PSCAD used to perform Fast Fourier Transform and symmetric component transform.

Another consideration is whether the analysis should be made in the sequence- or dq-domain. The common feature between the two is that they reduce the system dimension of a three-phase system, as long as the zero-sequence is neglected. Other than that, they differentiate in the way that the dq-domain provides higher accuracy for lower frequencies (ie. below $100\,\text{Hz}$) but also comes at the price of higher complexity. The sequence domain reduces the complexity but is also not as accurate for low-range frequencies. Since this thesis focuses on higher frequencies, it is assumed that the loss of accuracy at lower frequencies does not affect the results in a high manner. Therefore, the harmonic resonance analysis is performed in the sequence domain. As previously mentioned, the component in presented in figure 4.2.2 can be used to accomplish

this. The reader is referred back to Section 2.1 for the fundamentals of symmetrical components in power systems. For the reader's convenience, the symmetric component transform of phase voltages is given by the equation below. The reader is also reminded that the transform can be applied to currents as well. [55]

$$
\begin{bmatrix} V_0(f) \\ V_1(f) \\ V_2(f) \end{bmatrix} = \frac{1}{3} \cdot \begin{bmatrix} 1 & 1 & 1 \\ 1 & a & a^2 \\ 1 & a^2 & a \end{bmatrix} \begin{bmatrix} V_a(f) \\ V_b(f) \\ V_c(f) \end{bmatrix}
$$

$V_0$, $V_1$ and $V_2$ is the zero-, positive- and negative sequence components, respectively. $a$ is $1\underline{/120°}$ and $V_a$, $V_b$ and $V_c$ are the phase voltages. The inclusion of $f$ is to indicate that the the transform can be done for any frequency. Calculating the symmetrical voltage and current components facilitates the calculation of the harmonic impedance. It is assumed that the system is balanced, so the zero-sequence component is omitted. Additionally, for a balanced system, the positive sequence current at a given frequency only induces a corresponding positive sequence voltage for that same frequency. This means that the sequence components are decoupled, ie. they do not affect each other. The positive- and negative sequence impedances are given by equations 4.2.1 and 4.2.2. The impact of negative sequence is neglected in this thesis since positive sequence is the parameter providing the most relevant analysis [48]. If the symmetrical components are plotted against frequency, the frequency response of the converter is obtained. [55]

$$
Z_1(f) = \frac{V_1(f)}{I_1(f)} \tag{4.2.1}
$$

$$
Z_2(f) = \frac{V_2(f)}{I_2(f)} \tag{4.2.2}
$$

After the sequence components are calculated, the equivalent impedance of the grid, $Z_{\text{eq}}$, can be determined. Since the converter- and grid impedances are parallel to each other, this is achieved by using equation 4.2.3.

$$
Z_{\text{eq}} = \frac{1}{\frac{1}{Z_{\text{grid}}} + \frac{1}{Z_{\text{conv}}}} \tag{4.2.3}
$$

At this point, the harmonic instability results reveal potential active impedance behavior of the converter and how the frequency response of the converter affects the frequency response of the overall system, as shown in figure 2.5.5.

**Splitting of subsystems**

In order to further increase the validity of the frequency response of the converter, it is recommended to split the grid- and converter systems in two separate systems when conducting the current injection, as shown in figure 4.2.3. This is due to the high impedance of the converter relative to the grid. This high impedance forces large part of the injected current towards the grid. Consequently, large current injection amplitudes, ie. 50% of the RMS current and above, are necessary. Such a large injection amplitude may distort the resulting converter impedance, because part of the current flowing towards the grid may be reflected back towards the converter [48]. This is in opposition to the findings of [55], who discussed the implication of choice between current- and voltage perturbation.
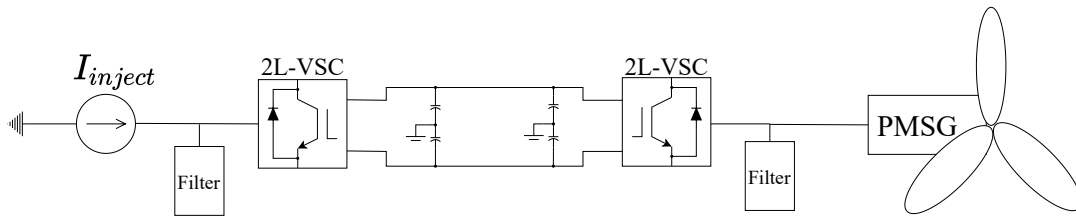


**Figure 4.2.3:** Current perturbation on isolated converter.

Before the harmonic currents are injected, the voltage signal on the filter output is measured and subject to FFT. The voltage waveforms and FFT results are presented in figure 4.2.4. It is observed that the voltage waveforms experience heavy distortion, despite being filtered. In order to verify if the voltage is too distorted, the THD is calculated and compared to the IEEE-519 standard. The resulting THD-calculation is presented in table 4.2.1. As previously mentioned, the standard states that the upper limit for $\text{THD}_V$ is 5% [47]. The THD calculated for the grid-side voltage profile of the isolated converter surpasses this limit. Consequently, the Harmonic Resonance Analysis is performed without splitting the system.

**Table 4.2.1:** THD calculation of voltage signal on the grid-side of the isolated converter.

| $\textbf{THD}_V$ | 32.4419 % |
|---|---|
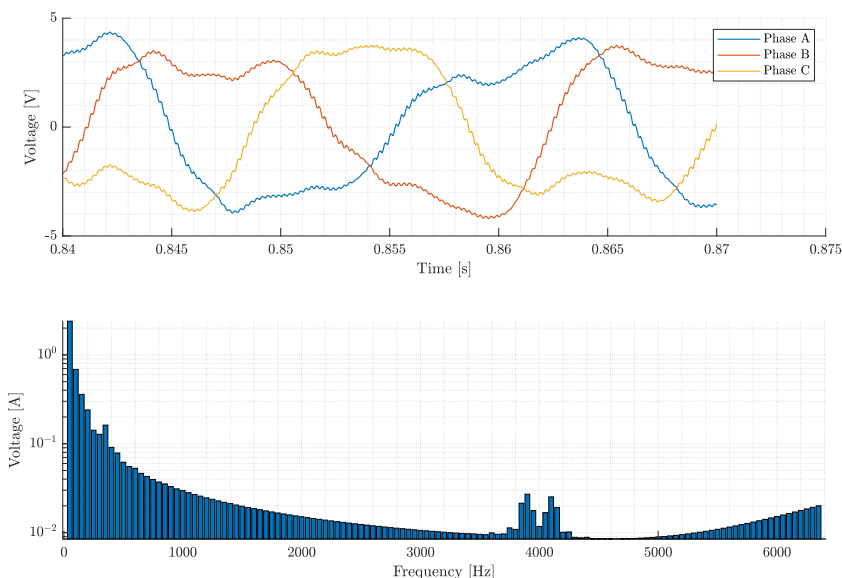


**Figure 4.2.4:** The figure presents the grid-side voltage profile of the isolated converter and the resulting FFT analysis of the signal.

# Chapter 5

# Harmonic Resonance Analysis Results

This chapter presents the results after performing harmonic resonance analysis on different systems and settings. A verification model with its impedance known is designed in order to be able to calculate its frequency response analytically. This analytical result is used to verify the numerical method. Once the method is verified, the grid-side converter described in Section 3.2 is subject to the numerical perturbation method described in Section 4.2. An important detail is that the LCL filter is included in this analysis. The converter impedance is then combined with the grid impedance in order to analyze the equivalent impedance of the system. Lastly, time delay is introduced to the current controller of the grid-side converter to investigate its effect on the converter frequency response.

## 5.1 Verification of Method

In order to test the numerical method, a model with known parameters is analyzed implementing said method. The numerical results are then compared to the analytical frequency response of the model in order to verify the numerical method. Figure 5.1.1 depicts a simple RL-circuit, acting as the verification model. Table 5.1.1 presents the values for each respective component in the model in addition to the implemented simulation parameters. The injected current magnitude is based on 5% of the measured RMS current.

**Table 5.1.1:** The parameters used in the verification model.

| Parameter | Value |
|---|---|
| Duration | $1\,\text{s}$ |
| Time Step | $10\,\mu\text{s}$ |
| $I_{\text{inj}}$ | $0.135\,\text{kA}$ |
| $V_{\text{Source}}$ | $230\,\text{kV},\ 50\,\text{Hz}$ |
| R | $0.65\ \Omega$ |
| L | $0.03\ \text{H}$ |

Figure 5.1.2 presents the numerical- and analytical results of the frequency response of the verification model. It is observed that the numerical magnitude matches the analytical magnitude. In addition, the magnitudes are increasing for higher frequencies, which is the characteristic of an inductive circuit. Regarding the phase angle, the analytical result approaches 90°. The phase angle for the numerical method however fluctuates greatly around 90°.
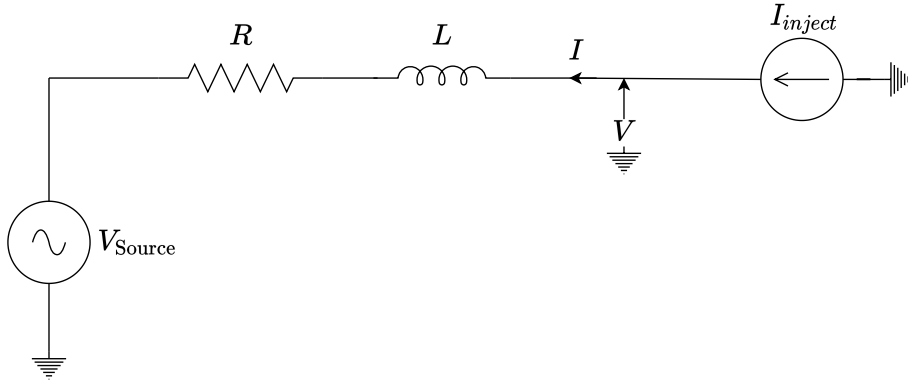
**Figure 5.1.1:** Model with known impedance used to verify method of deriving impedance.
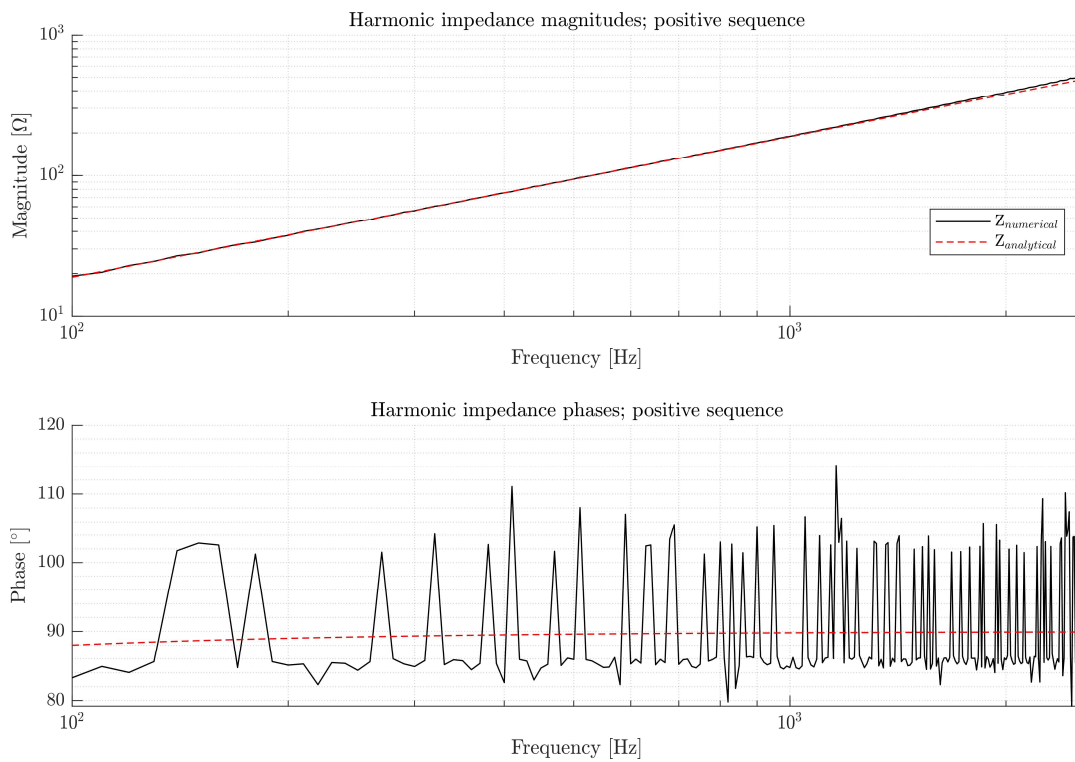


**Figure 5.1.2:** The numerical- and analytical approach of deriving the frequency response of the verification model.

## 5.2 Impedance Equivalent of 2L-VSC

Table 5.2.1 presents the input parameters used to acquire the frequency response of the converter. The measured RMS current at the LCL filter-output is 1.7 kA, which makes the magnitude of the injected current equal to 117% of the RMS current. As is described in Section 4.2, the recommended current amplitude should be between 1-10%, which is not the case here. The reason for this is stated in Section 4.2. The resulting frequency response of the converter is illustrated in figure 5.2.1. The phase angle includes two red areas, indicating the thresholds of negative damping. It is observed that the magnitude is increasing up to approximately 900 Hz, exhibiting inductive behavior, before starting to decrease for higher frequencies, which is capacitive behavior. The phase angle lies at 90° up to 300 Hz, before starting to decrease for higher frequencies and looks to be stabilizing at -90°. These results indicate that the frequency response follows the installed LCL filter which has a cutoff frequency at 900 Hz, which is capacitive for higher frequencies. It is also observed a high degree of fluctuation in both phase angle and magnitude for lower frequencies. The phase angle crosses the negative damping threshold between 100 Hz and 350 Hz, but this may be due to the aforementioned fluctuation.

**Table 5.2.1:** Input parameters implemented in converter impedance derivation.

| Parameter | Value |
|---|---|
| Duration | 1 s |
| Time Step | 10 $\mu$s |
| $I_{RMS}$ | 1.7 kA |
| $I_{inj}$ | 3.7 kA |
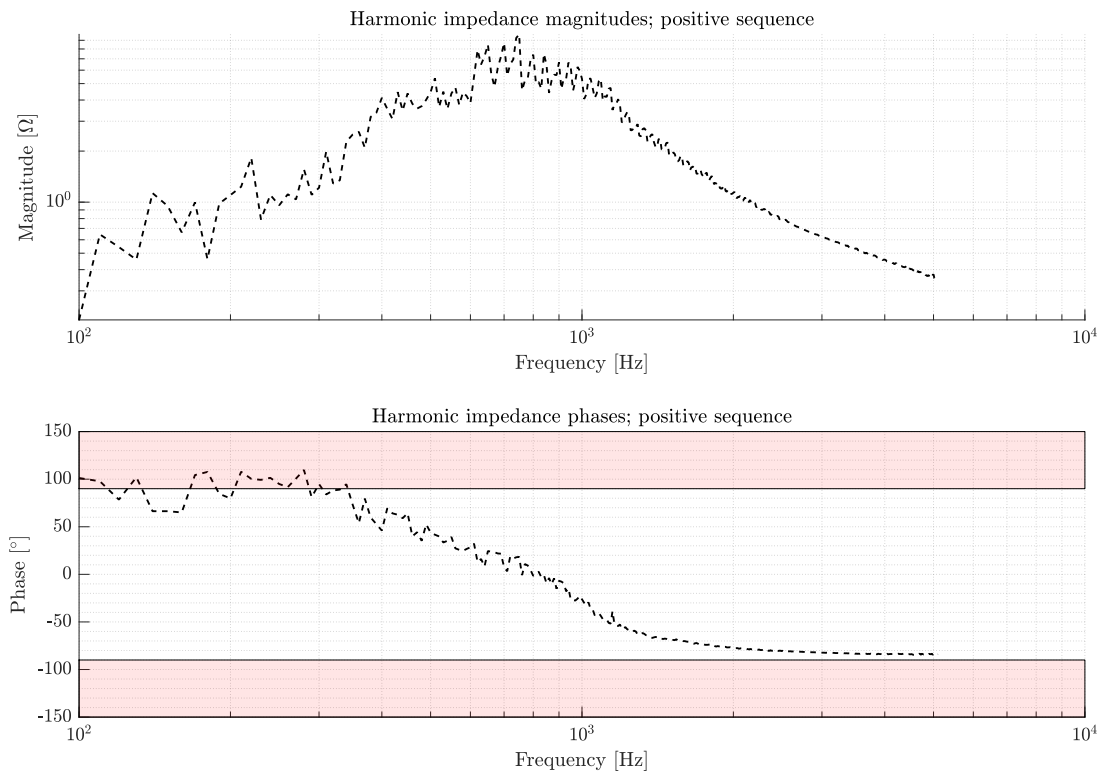


**Figure 5.2.1:** The figure presents the frequency response of the grid-side converter. The phase angle figure includes two red areas indicating negative damping.

In order to illustrate the results when the injected harmonic current amplitude follows the theoretical recommendation, figure 5.2.2 is included. Table 5.2.2 presents the input parameters of the simulation. As can be seen in the table, the injected current amplitude is set to 0.085 kA, which is equivalent to 5% of the measured RMS current. The figure clearly shows large fluctuations in the low-frequency range and is testimony to why large amplitudes of the injected harmonic currents are necessary when the converter can not be an isolated subsystem, as discussed in Section 4.2.

**Table 5.2.2:** Input parameters implemented in converter impedance derivation where the injection amplitude follows the recommended value found in literature.

| Parameter | Value |
|-----------|-------|
| Duration | 1 s |
| Time Step | $10\,\mu s$ |
| $I_{RMS}$ | 1.7 kA |
| $I_{inj}$ | 0.085 kA |
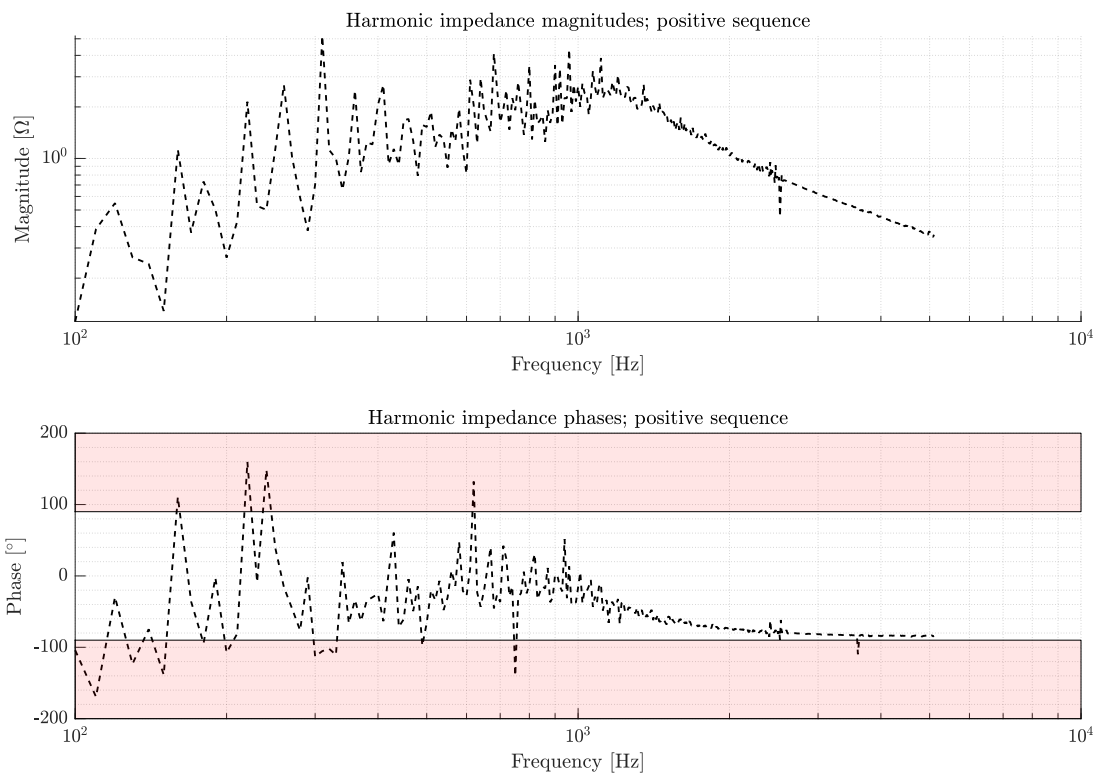


**Figure 5.2.2:** The figure presents the frequency response of the grid-side converter where the injection amplitude follows the recommended value found in literature. The phase angle figure includes two red areas indicating negative damping.

## 5.3    Impedance Equivalent of Wind Farm

Harmonic Resonance Analysis entails analyzing the interaction between the connected converter and the grid, as described in Section 2.5.2. Table 5.3.1 presents the input parameters when analyzing the grid connected to one string. The magnitudes of the harmonic currents injected towards the grid and converter equal to 5.9% and 117%, respectively. Figure 5.3.1 depicts the converter-, grid- and equivalent impedances. As explained in Section 2.5.2, the intersections between the converter- and grid impedances determine the parallel resonances of the equivalent impedance. The phase difference at the intersections determine the damping of the resonance, the closer the difference is to 180°, the less damping is present. The results reveal parallel resonances at $710\,\text{Hz}$ and $3\,960\,\text{Hz}$, highlighted by the red lines. The difference in phase angle at $710\,\text{Hz}$ is 1.3°, while it is 178° at $3\,960\,\text{Hz}$. As can be seen by the magnitudes, the system experiences more damping at the first resonance. However, for the resonance at $3\,960\,\text{Hz}$, there is not much damping. Consequently, the equivalent resonance far exceeds the converter- and grid magnitudes. Additionally to the parallel resonances, there is one series resonance at $1\,000\,\text{Hz}$.

**Table 5.3.1:** Input parameters implemented in deriving frequency response of single-string OWF.

| Parameter | Value |
|---|---|
| Number of turbines | 1 |
| Duration | $1\,\text{s}$ |
| Time Step | $10\,\mu\text{s}$ |
| $I_{\text{RMS}}$ | $1.7\,\text{kA}$ |
| $I_{\text{inj,conv}}$ | $3.7\,\text{kA}$ |
| $I_{\text{inj,grid}}$ | $0.1\,\text{kA}$ |
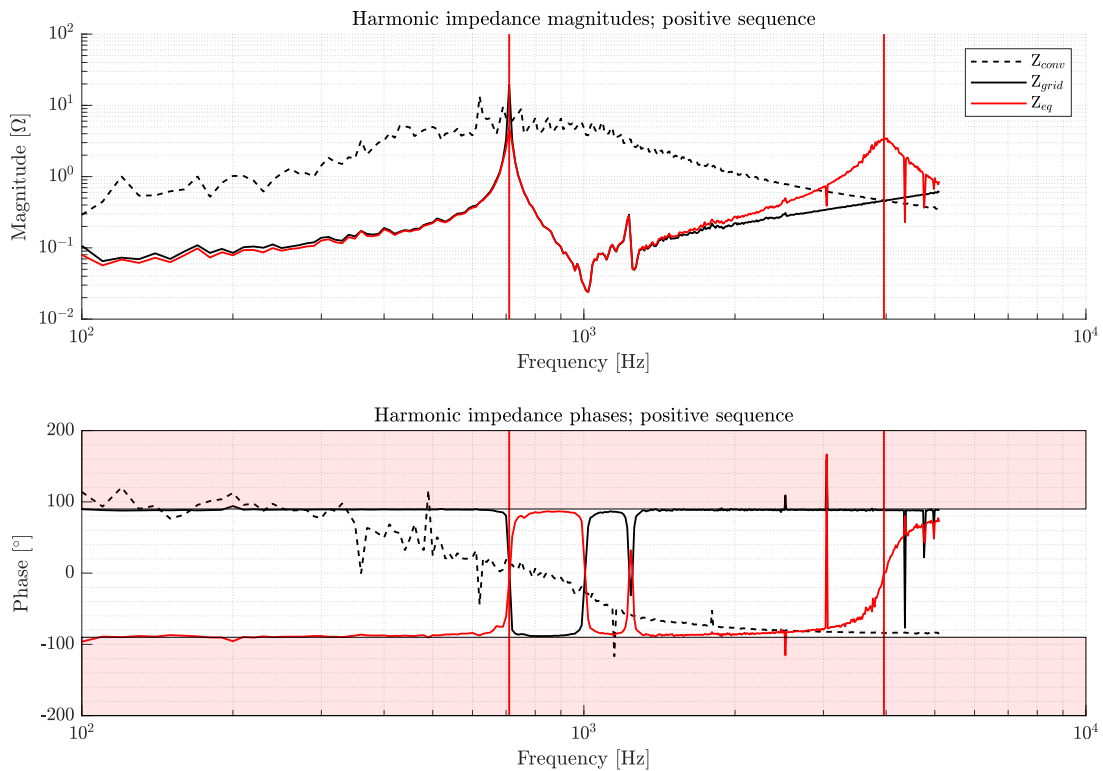


**Figure 5.3.1:** The figure depicts the frequency responses of the grid and converter for a single string. The equivalent impedance is also included.

Table 5.3.2 displays the simulation parameters implemented when analyzing 100 strings connected. Figure 5.3.2 presents the frequency response of the converter and grid together with the calculated equivalent impedance. The red lines are placed at frequencies where the converter- and grid impedance magnitudes intersect. When the number of strings are increased, the collection grid consisting of cables and transformers also increase. This introduces more capacitance and inductance to the circuit, which lowers the resonance frequency of the grid. This is coherent with equation 2.2.8. By comparing figures 5.3.1 and 5.3.2 this is confirmed. It is observed that the first parallel resonance in the grid occurs at a much lower frequency, which affects the frequency the intersection between the grid- and converter impedances takes place. In this case, that intersection occurs at 280 Hz, which is a substantial decrease when compared to the single-string wind farm. It is also observed that the series resonance occurs at 800 Hz, which is 200 Hz lower than when one single string was connected. The highest frequency intersection occurs at the same frequency as with one string.

**Table 5.3.2:** Input parameters implemented in converter impedance derivation when 100 strings are connected.

| Parameter | Value |
|---|---|
| Number of turbines | 100 |
| Duration | 1 s |
| Time Step | 10 $\mu$s |
| $I_{RMS}$ | 1.7 kA |
| $I_{inj,conv}$ | 3.7 kA |
| $I_{inj,grid}$ | 0.03 kA |
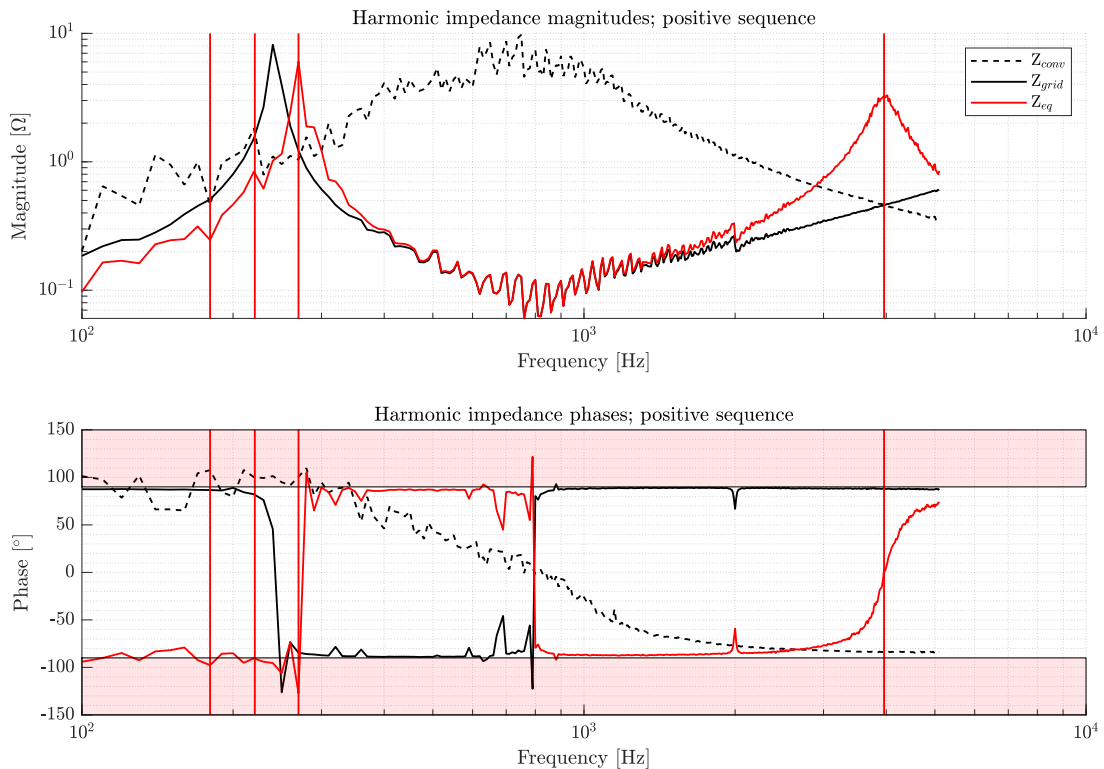


**Figure 5.3.2:** The figure depicts the frequency responses of the grid and converter when 100 strings are connected. The equivalent impedance is also included.

## 5.4　Introducing Time Delay to Current Controller

According to the literature study in Section 2.6, introducing a time delay in the current controller causes the phase angle to cross the negative damping threshold. In this section, a time delay is introduced on the three-phase current signal prior to the Park-transform, shown in figure 3.2.4. Consequently, the time delay has the largest repercussions. In this section, two cases where time delay has been introduced are presented. The first case utilizes a time delay equal to $200\,\mu s$. In the second case, a time delay of $400\,\mu s$ is implemented. Table 5.4.1 summarizes the input parameters used when deriving the converter- and grid impedances in the first case. Figure 5.4.1 displays the converter-, grid and equivalent impedances for the first case. When comparing this case to figure 5.4.2, where no time delay is implemented, no real difference, or negative damping, is observed.

**Table 5.4.1:** Input parameters implemented in deriving the frequency response of a single-string OWF. In addition, a time delay of $200\,\mu s$ is introduced in the Current Controller.

| Parameter | Value |
|---|---|
| Number of turbines | 1 |
| Duration | $1\,s$ |
| Time Step | $10\,\mu s$ |
| $I_{RMS}$ | $1.7\,kA$ |
| $I_{inj,conv}$ | $3.7\,kA$ |
| $I_{inj,grid}$ | $0.1\,kA$ |
| Time Delay | $200\,\mu s$ |
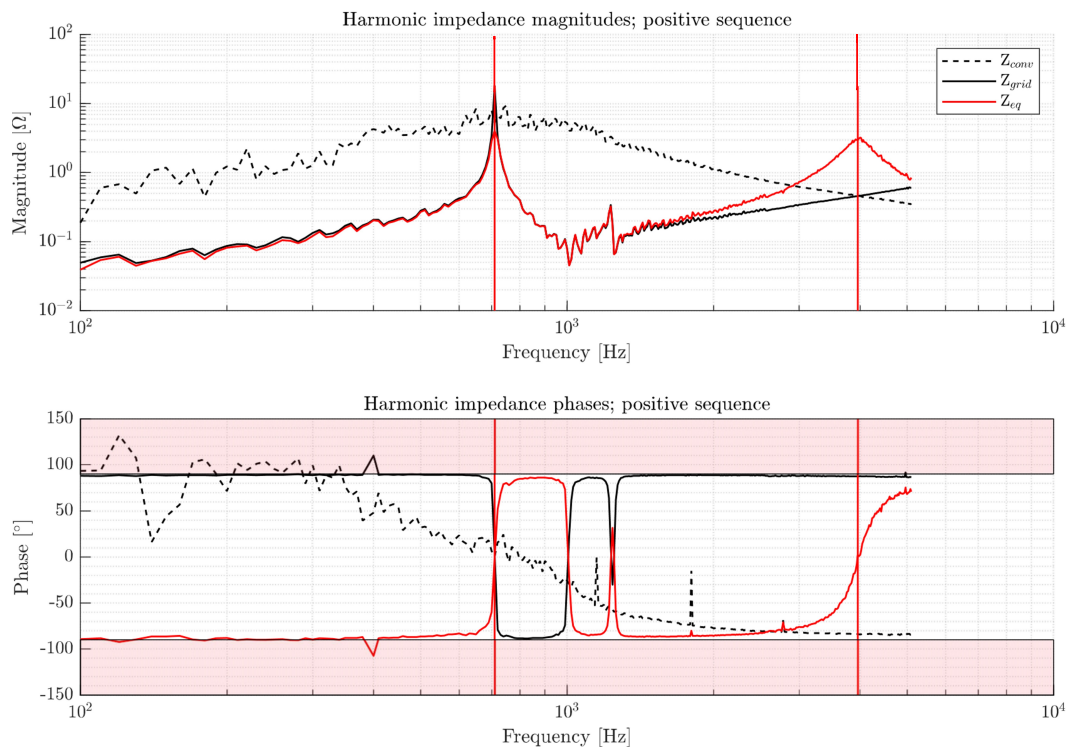


**Figure 5.4.1:** The figure depicts the frequency responses of the grid and converter when one single string is connected and a time delay of $200\,\mu s$ is implemented. The equivalent impedance is also included.

In order to try to provoke negative damping, the time delay is increased to $400\,\mu$s. The input parameters used in the simulation is summarized in table 5.4.2, and figure 5.4.2 presents the simulation results. According to the results, the introduction of a time delay did not introduce negative damping or other changes to the frequency response.

As reported by [42], if the system experienced negative damping in the case with $200\,\mu$s delay, then the negative damping would appear at a lower frequency with the delay implemented set to $400\,\mu$s. If this negative damping coincided with a resonance frequency, this would cause the converter to continuously emit harmonic components and eventually trip the protection system.

**Table 5.4.2:** Input parameters implemented in deriving frequency response of single-string OWF. In addition, a time delay of $400\,\mu$s is introduced in the Current Controller.

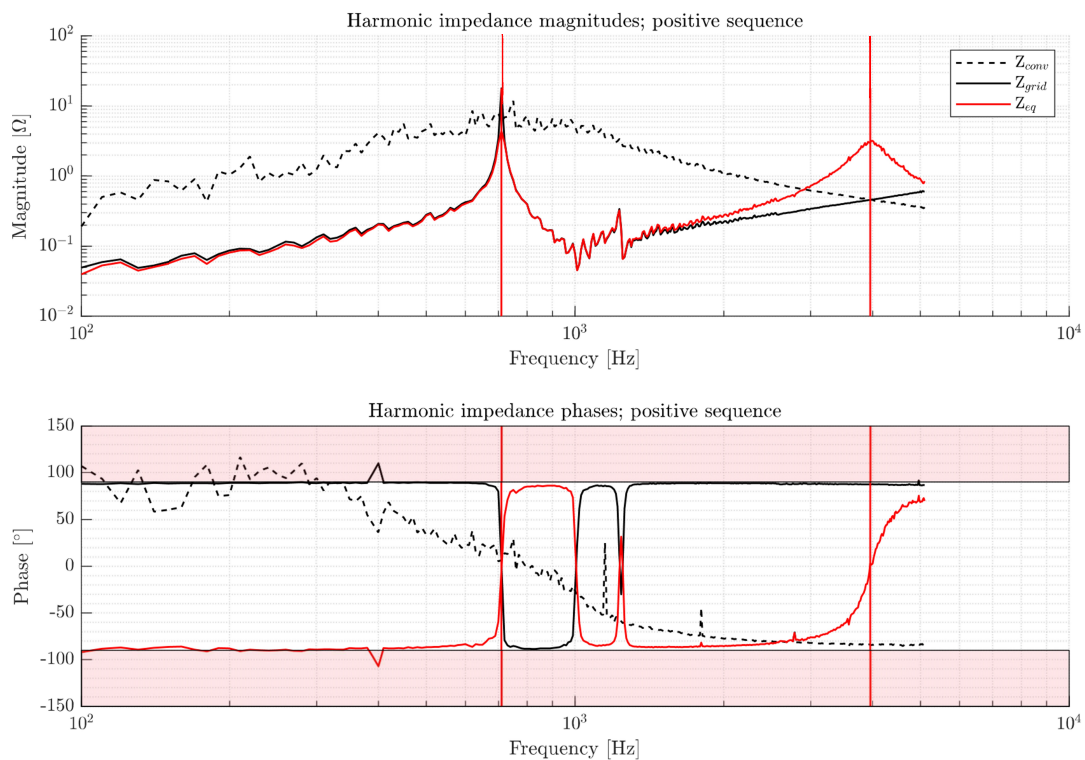| Parameter | Value |
|---|---|
| Number of turbines | 1 |
| Duration | $1\,$s |
| Time Step | $10\,\mu$s |
| $I_{inj,conv}$ | $3.7\,$kA |
| $I_{inj,grid}$ | $0.1\,$kA |
| Time Delay | $400\,\mu$s |



**Figure 5.4.2:** The figure depicts the frequency responses of the grid and converter when one single string is connected and a time delay of $400\,\mu$s is implemented. The equivalent impedance is also included.

# Chapter 6

# Discussion

## 6.1 Model impact on Harmonic Resonance Analysis quality

In order to derive the converter impedance, the voltage- and current signals at the filter output prior to the perturbation has to be of high quality. A low current ripple demands sufficient design of the converter inductor while a low voltage distortion depends on the filter design, as shown in sections 3.2.1 and 3.3, respectively. According to the standard set by IEEE-519-2014, the Total Harmonic Distortion of both the voltage- and current signals are far beneath the limits, but some distortion is still present. It is impossible to ascertain how much this distortion affects the Harmonic Resonance Analysis results, but since the THD percentiles are both below 1%, it is possible that the present distortion does not have a big impact. Another factor affecting the harmonic emission from the converter is the switching frequency. An increase in switching frequency decreases the harmonic emission. For a 2L-VSC, the switching frequency is relatively low compared to converters utilizing switching between a higher number of voltage levels, such as the MMC. In order to decrease the harmonic emission further is to implement a 3L-VSC, which would decrease the need for the LCL filter, although not entirely. This may be beneficial related to Harmonic Resonance problems.

As described in Section 3.4, each string contains a simplified cable model at 5 km. This most likely affects the Harmonic Resonance Analysis and would deviate from implementing a more precise model. Although, the motivation for this thesis is not to replicate an already existing OWF, but to illustrate the interactions between the WTG's converter and the grid. A simplified cable model is sufficient to be able to illustrate the relevant phenomenons.

## 6.2 Verification of the Numerical Method

A weakness of the work done in this thesis is the absence of an analytical equivalent to the converter controller in order to verify the numerical results. This is a common denominator between other research performed within this field. Without this verification, there is no real way to be sure how accurate the results are. To counteract this source of uncertainty, the verification model shown in Section 5.1 is made. The verification model both fortifies the quality of the numerical method and reveals possible weaknesses of the method. As can be seen by the results, the magnitude of the impedance derived by the numerical method matches the impedance calculated by the analytical model. At the same time, the uncertainties of the numerical method is revealed in the phase angle plot. The analytical model acts as suspected and pushes closer to 90° at higher frequencies, while the numerical results fluctuates greatly around 90° with high peaks and low bottoms. This implies that the method is more accurate at deriving the impedance magnitudes and that it reveals the general trend for the phase angles.

In addition to an analytical model, an experimental setup would help verify the method. It would be very beneficial to be able to derive the frequency response of a physical system.

## 6.3 Fluctuation of Harmonic Resonance Results in Low-Frequency Range

A common denominator for the Harmonic Resonance Analysis performed in this thesis is the high degree of fluctuation of the converter impedance in the low-frequency range. Throughout the simulations, the largest impact on the impedance derivation was the injected harmonic current amplitudes. This suggests that the choice of amplitude may be a root cause for the fluctuation problem. Injecting the amplitude that yielded the best results was one of the main challenges during the simulations. The approach to achieving the presented results was based on trial and error, where different amplitudes were injected. The only guidelines to choosing the correct amplitude is that it should be in the range of 1-10% of the measured RMS current at the injection point. Although, this is only the case when it is possible to split the subsystems, as elaborated on in Section 4.2. In this thesis, this was not possible. The solution to this problem was to run separate simulations for the derivation of the grid- and converter impedances. For the grid impedance, it is possible to get an approximation of the most suitable harmonic amplitude by following the aforementioned guideline. For the converter impedance, however, this is not the case because of the high impedance of the converter related to the grid. For a given amount of current injected, only a fraction flows towards the converter. Consequently, the injected amplitude has to be high to ensure a sufficient flow towards the converter. Although, this may be a source of error. When injecting a large amplitude, the current flowing towards the grid may be reflected back towards the converter, which may distort the converter frequency response. This may be the reason for the fluctuation in the harmonic resonance results in the low-frequency range.

A possible solution to this problem may be to split the system. This would remove or reduce the challenges related to the tuning of the injection current and the reflected current flowing from the grid towards the converter. In order to split the system, the distorted voltage profile at the filter output has to be dealt with. It is unknown why the voltage profile experiences such high distortion, but possible reasons may be insufficient filter design for the case where the converter is isolated.

Another source of error is the design of the converter controller. The controller is designed by [43], which makes total insight into the dynamics impossible. Because of this, it may be part of the reason why the voltage profile experiences a high degree of distortion since it may be designed with only a certain number of operation points in mind.

## 6.4 Impact of Control Parameters

According to the literature study in Section 2.6, the control parameters of the converter affects the converter impedance. More specifically, introducing time delays in the current controller causes the converter phase angle to cross the negative damping threshold. This thesis attempts at highlighting this phenomenon in Section 5.4, but no negative damping was achieved. The reason for this is unclear, but four possibilities are discussed:

- uncertainties related to the control design

- uncertainties related to the design of LCL filter

- magnitude of injected harmonic currents

- limitations set in PSCAD

As described in Section 3.2.2, the controller is designed by [43]. This makes any results dependent on the controller an uncertainty, since it may be developed to counteract behavior that is normally regarded as unwanted, but regarded as desired in this thesis. It is a possibility that the controller is designed to have active damping, which would alter the impedance based on measurements, although, this is not mentioned in the documentation or is found anywhere in the controller. A clear advantage would have been to design and tune the controller. This would make the controller performance easier to predict.

The design of the LCL filter is also based on [43]. The design process and resulting effectiveness of the filter is highlighted in Section 3.3. As illustrated in figure 3.3.2, the implementation of the filter has a clear effect on the voltage harmonics, but the design procedure of the filter parameters is not similar to anything found in literature. This creates some uncertainties related to the results dependent on the filter.

Again, the amplitude of the injected harmonic currents may have effects that are not easy to predict. It is definitely a flaw of the numerical method and may impact the frequency response in unpredictable manners.

There may be sources of error within PSCAD. As described in Section 4.2, PSCAD is used in performing both the symmetrical component transformation and the Fast Fourier Transform. Both of these transformations are executed by a common component. Although the component has its own documentation, it is a component that does not enable the user to observe the intermediate calculations. This leaves the user to having no alternative but to trust the output. It may have been beneficial to confirm the results in another simulation software, eg. Matlab, but this was deemed too time intensive.

## 6.5   Harmonic Resonance and Different System Topologies

A resonance frequency is formed when the magnitude of the converter- and grid impedances intersect. The difference in phase angles decides the damping of the resonance. This is further elaborated on in Section 2.5.2. For a system operator, the intersection between these magnitudes and how it can be altered may be valuable information. In addition, information on how to best introduce damping at respective resonances may be beneficial. It is shown in this thesis that the 2L-VSC converter impedance has a frequency response of an inductor up to the cutoff frequency of the implemented LCL filter, and of a capacitor for higher frequencies. This information may be beneficial when deciding key design aspects of the OWF, such as size of the collector grid and the transmission system to the onshore grid. If this information is evaluated together with the converter controller, it may be possible to get an idea how the converter- and grid impedances interact.

The cutoff frequency of the filter decides what frequency the filter starts having negative gain, ie. what harmonic components are filtered out. It is important to filter out a sufficient amount of harmonics in order to comply with the harmonic limits standards set by IEEE-519-2014, but this also affects the frequency response of the converter. Applying a low cutoff frequency provides a smooth voltage profile, but it also creates a capacitive converter in the low-frequency range. If this is combined with a system that has a frequency response of an inductor in the same frequency range, this may create an intersection between the converter- and grid impedances.

An example of this is overhead transmission lines. Due to the alternating current flowing through them, they experience a magnetic field around them. This provides them with an inductive property at low frequencies. In this thesis, transmission by overhead lines to the onshore grid is the chosen option in contrast to subsea cables. The reasoning behind this decision was the

simplicity overhead lines brought with it.

In a more realistic example, subsea cables would probably be the chosen transmission option. By implementing cables, the grid would be introduced with a larger capacitance which further would lower the resonance frequency of the grid. Consequently, the first resonance would occur in the low-frequency range.

This is also seen when the size of the collector system is increased. Increasing the collector grid introduces the grid to more cables and transformers, further decreasing the resonance of the grid impedance and will most likely result in a low-frequency intersection between the converter- and grid impedance magnitudes, as shown in figure 5.3.2. On the other hand, increasing the amount of cables also increases the resistive damping at high frequencies[48], which is beneficial regarding resonances at higher frequencies and harmonic components at those respective frequencies.

Another possible topology is the Type-IV wind turbine connected to the onshore grid my MMC-HVDC transmission. As previously mentioned, the filter capacitor at the 2L-VSC output dominates the impedance at frequencies above the filter's cutoff frequency, making it capacitive. For a Modular Multilevel Converter, however, the opposite is true. Due to the arm reactor, the MMC exhibits inductive impedance at high frequencies. This enables a possible crossing between the impedances of the two converters in the high-frequency ranges.

Once the intersections yielding a resonance between the converter- and grid impedances have been considered, another important aspect to take into regard is the potential negative damping of the converter. As explained in Section 2.6, an increase in time delay results in negative damping at lower frequencies. If the given topology is like the one presented in this thesis and the number of strings are set to 100, the first parallel resonance is probably located in the low-frequency range. If the time delay of the converter controller is high enough, this resonance can coincide with the negative damping region. This would result in continuous emission of the harmonic components located within this resonance. Consequently, unstable operation would ensue and the protection system would trip. This potential interaction demands attention and underlines the need for Harmonic Resonance Analysis, which makes the numerical perturbation method described in this thesis a valuable tool. Although, it is contingent on the quality of the model since every model does not reveal its negative damping regions.

As explained in Section 2.3, passive- and active damping can be implemented in order to introduce damping to the system. The active damper could be implemented inside the converter controller in order to prevent unwanted impedance behavior. The passive damper would introduce a more inefficient system, due to the increase in active power losses. It could also be used to alter a discovered resonance that coincides with a negative resistance frequency range. This would perhaps prove to be a challenge, since the system operation conditions, ie. number of turbines in operation, may change over time.

# Chapter 7

# Conclusion & Further Work

## 7.1 Conclusion

This thesis investigates how to utilize the numerical Current/Voltage Perturbation Method in order to derive the frequency response of a converter. The interaction between the converter- and grid impedances is then examined by performing Harmonic Resonance Analysis. Lastly, the impact of controller parameters on the converter impedance is explored.

It is found that the numerical method can be used to successfully determine the converter impedance. It is therefore a valuable tool for a system operator who rarely have full insight into the control parameters of the converters supplied to them by the manufacturers. Although, because of a high degree of fluctuation in the low-frequency range, there are some uncertainties related to the results.

The results from the Harmonic Resonance Analysis yields the interaction between the converter- and grid impedances. It is revealed that, depending on the difference in phase angles, the intersection between the magnitudes of the converter- and grid impedances results in an equivalent resonance frequency. In addition, by comparing a single-string wind farm to that of a 100-string wind farm, it is found that the expansion of the collector grid reduces the first equivalent parallel resonance between the converter- and grid impedances. For the single-string wind farm, the first equivalent parallel resonance frequency is found to occur at 710 Hz. Although, when the number of strings are increased to 100, the corresponding resonance frequency occurs at 280 Hz. This implies that the stability regions of a system is heavily dependent on the system topology. The impact of filter parameters and how different system topologies may affect the equivalent harmonic resonances is also discussed.

Time delays are introduced in the current controller in an attempt to reveal the negative damping phenomenon of the converter. This was unsuccessful. The most probable reason for the failed attempt is the use of an already existing controller model made by PSCAD. The controller may be designed to counteract what normally would be regarded as unwanted behavior, that would in this thesis be regarded as wanted behavior. If the controller was built from the bottom, this may have been prevented.

## 7.2 Further Work

Further extensions to the project could be implemented if the time frame of the thesis was extended. First of all, the design of the converter controller should be revised. It should either be built from the ground up or heavily studied in order to fully understand its dynamic behavior. Furthermore, one of the weaknesses of this thesis is the lack of a proper comparative model. This would be solved by modeling an analytical equivalent of the converter and grid. This would verify the numerical results in a much greater deal than that of the verification model proposed in this thesis. Additionally, an experimental setup would be a good addition to this research work in order to investigate if the method is implementable in a real system. This would also enable comparing the alternative methodologies proposed in academia related to harmonic interactions. Consequently, evidence on which approach provides the best results would be available. Lastly, a study where active- and/or passive damping is implemented to mitigate harmonic resonance issues would be interesting.

# Bibliography

[1] Anders Fjeldberg Teigmoen. *Harmonics and Resonances in Offshore Wind Farms.* (Accessed on 01/02/2021). Dec. 2020.

[2] Olimpo Anaya-Lara et al. *Offshore Wind Energy Technology.* eng. First. 2018. ISBN: 9781119097808.

[3] Anders Teigmoen and Kristian Husmo Lyngved. *Technologies for Offshore Wind Transmission.* (Accessed on 11/11/2020). Nov. 2020.

[4] Chong Ng and Li Ran. *Offshore Wind Farms - Technologies Design and Operation.* eng. First. 2016. ISBN: 978-0-08-100779-2.

[5] Thomas Ackermann. *Wind Power in power Systems.* eng. First. 2012. ISBN: 978-0-470-97416-2.

[6] Gregor Giebel and Tuhfe Göçmen. *Estimation of turbulence intensity using rotor effective wind speed in Lillgrund and Horns Rev-I offshore wind farms.* (Accessed on 30/10/2020). June 2016. URL: https://www.researchgate.net/publication/305810655_Estimation_of_turbulence_intensity_using_rotor_effective_wind_speed_in_Lillgrund_and_Horns_Rev-I_offshore_wind_farms.

[7] Jakob Glasdam et al. *Review on Multi-Level Voltage Source Converter Based HVDC Technologies for Grid Connection of Large Offshore Wind Farms.* (Accessed on 15/10/2020). Oct. 2012. URL: https://ieeexplore.ieee.org/stamp/stamp.jsp?arnumber=6401377.

[8] ALSTROM. *Microsoft PowerPoint - LCC vs VSC.* (Accessed on 11/15/2020). URL: https://sari-energy.org/oldsite/PageFiles/What_We_Do/activities/HVDC_Training/Presentations/Day_7/LCC_vs_VSC_ALSTOM.pdf.

[9] Nadja Skopljak. *Albatros Goes Into Operation.* (Accessed on 30/10/2020). Jan. 2020. URL: https://www.offshorewind.biz/2020/01/10/albatros-goes-into-operation/.

[10] Adnan Durakovic. *Global Tech I at Full Tilt.* (Accessed on 30/10/2020). Dec. 2019. URL: https://www.offshorewind.biz/2019/12/25/global-tech-i-at-full-tilt/.

[11] Veja Nate. *Veja Mate delivers first power from the North Sea.* (Accessed on 30/10/2020). Jan. 2017. URL: http://www.vejamate.net/blog/2017/1/16/veja-mate-delivers-first-power-from-the-north-sea.

[12] TenneT. *BorWin2.* (Accessed on 30/10/2020). URL: https://www.tennet.eu/our-grid/offshore-projects-germany/borwin2/.

[13] J. Duncan Glover, Mulukutla S. Sarma, and Thomas J. Overbye. *Power System Analysis and Design.* eng. Fifth. 2012. ISBN: 978-1-111-42577-7.

[14] Francisco C. De La Rosa. *Harmonics and Power Systems.* eng. First. 2006. ISBN: 9780429126369.

[15] Jos Arrillaga and Neville R. Watson. *Power System Harmonics.* eng. Second. 2003. ISBN: 978-0-470-85129-6.

[16] Kalle Rauma. "Electrical Resonances and Harmonics in a Wind Power Plant". (Accessed on 01/11/2020). MA thesis. Aalto University, Feb. 2012.

[17]  Emmanuel Hernandez et al. *Fourier Transforms High-tech Application and Current Trend*. eng. First. 2017. ISBN: 978-953-51-2894-6.

[18]  David Morin. *Waves - Fourier Analysis*. (Accessed on 29/10/2020). Nov. 2009. URL: `https://scholar.harvard.edu/david-morin/waves`.

[19]  L&T Switchgear. *Understanding Current & Voltage Harmonics*. (Accessed on 05/31/2020).

[20]  Łukasz Hubert Kocewiak, Jesper Hjerrild, and C.L. Bak. *Harmonic models of a back-to-back converter in large offshore wind farms compared with measurement data*. (Accessed on 15/10/2020). Jan. 2009. URL: `https://www.researchgate.net/publication/242728877_Harmonic_models_of_a_back-to-back_converter_in_large_offshore_wind_farms_compared_with_measurement_data`.

[21]  Zubair Ahmed Memon, Mohammad Aslam Uquaili, and Mukhitiar Ali Unar. *Harmonics Mitigation of Industrial Power System Using Passive Filters*. (Accessed on 20/04/2021). Mar. 2012. URL: `https://arxiv.org/ftp/arxiv/papers/1605/1605.06684.pdf`.

[22]  Hussein A. Kazem. *Harmonic Mitigation Techniques Applied to Power Distribution Networks*. (Accessed on 20/04/2021). Feb. 2013. URL: `https://www.hindawi.com/journals/ape/2013/591680/`.

[23]  Jian Sun. *Passive Methods to Damp AC Power System Resonance Involving Power Electronics*. (Accessed on 05/15/2021). July 2018. URL: `https://ieeexplore.ieee.org/document/8460076`.

[24]  Salvatore D'Arco. *Basics of Compensation and Harmonic Filtering - PowerPoint slide 19*. (Accessed on 1/12/2020). Nov. 2020.

[25]  M. Bradt et al. *Harmonics and resonance issues in wind power plants*. (Accessed on 07/11/2020). June 2011. URL: `https://ieeexplore.ieee.org/document/6039398`.

[26]  Aleksandr Reznik et al. *LCL Filter Design and Performance Analysis for Grid-Interconnected Systems*. (Accessed on 05/06/2021). June 2013. URL: `https://ieeexplore.ieee.org/document/6571219`.

[27]  Ryszard Klempka. *A New Method for the C-Type Passive Filter Design*. (Accessed on 20/04/2021). June 2012. URL: `https://www.researchgate.net/publication/265964333_A_New_Method_for_the_C-Type_Passive_Filter_Design`.

[28]  Henrik Brantsæter et al. *Passive Filter Design and Offshore Wind Turbine Modelling for System Level Harmonic Studies*. (Accessed on 04/03/2021). Dec. 2015. URL: `https://www.sciencedirect.com/science/article/pii/S1876610215021761`.

[29]  Stephen Gergely and David Crecraft. *Analog Electronics: Circuits, Systems and Signal Processing*. eng. First. 2002. ISBN: 978-0750650953.

[30]  Qiang Sun et al. *Design of Active Power Filter for Low Voltage and High Current Switching Power Supply*. (Accessed on 09/11/2020). Mar. 2011. URL: `https://ieeexplore.ieee.org/document/5749130`.

[31]  Wei Zhao, Zhou Shangli, and An Luo. *A New Injection Type Hybrid Active Power Filter and its Application*. (Accessed on 09/11/2020). Jan. 2011. URL: `https://ieeexplore.ieee.org/document/5720747`.

[32]  Mohammad A.S. Masoum and Ewald F. Fuchs. *Power Quality in Power Systems and Electrical Machines*. eng. Second. 2015. ISBN: 978-0-12-800782-2.

[33]  Syed M. Islam. *Characteristic and Non-Characteristic Harmonics, Harmonic Cancellations and Relevant International Standards in Variable Speed Drives*. (Accessed on 15/10/2020). June 2002. URL: `https://www.researchgate.net/publication/266355071_Characteristic_and_Non-Characteristic_Harmonics_Harmonic_Cancellations_and_Relevant_International_Standards_in_Variable_Speed_Drives`.

[34] Kamran Sharifabadi et al. *Design, Control, and Application of Modular Multilevel Converters for HVDC Transmission Systems.* eng. First. 2016. ISBN: 978-1-118-85156-2.

[35] Hansk Kristian Høidalen and R. Sporild. *Using Zigzag Transformers with Phase-shift to reduce Harmonics in AC-DC Systems.* (Accessed on 06/11/2020). Jan. 2005. URL: `https://www.researchgate.net/publication/229005021_Using_Zigzag_Transformers_with_Phase-shift_to_reduce_Harmonics_in_AC-DC_Systems`.

[36] Alexander Kusko and Marc T. Thompson. *Power Quality in Electrical Systems.* eng. First. 2007. ISBN: 9780071470759.

[37] CIGRE. *AC side harmonics and appropriate harmonic limits for VSC HVDC.* Tech. rep. CIGRE, 2019.

[38] Łukasz Kocewiak et al. (Accessed on 11/03/2020). Nov. 2020. URL: `http://www.lukasz.kocewiak.eu/index.php?language=en&page=publications`.

[39] Luca Bessegato et al. *Effects of Control on the AC-Side Admittance of a Modular Multilevel Converter.* (Accessed on 03/02/2020). Oct. 2018. URL: `https://ieeexplore.ieee.org/document/8514034`.

[40] Hani Saad et al. *On Resonances and Harmonics in HVDC-MMC Station Connected to AC Grid.* (Accessed on 10/07/2020). Jan. 2017. URL: `https://ieeexplore.ieee.org/document/7807345`.

[41] Bo Pang, Heng Niam, and Yunyang Xu. *Mechanism Analysis and Damping Method for High Frequency Resonance Between VSC-HVDC and the Wind Farm.* (Accessed on 05/07/2021). Sept. 2020. URL: `https://ieeexplore.ieee.org/document/9195160`.

[42] Jianguo Wang et al. *Delay-Dependent Stability of Single-Loop Controlled Grid-Connected Inverters with LCL Filters.* (Accessed on 05/10/2021). Feb. 2015. URL: `https://ieeexplore.ieee.org/document/7036119`.

[43] PSCAD. *Type 4 Wind Turbine Generators.* (Accessed on 02/11/2021). May 2018. URL: `https://www.pscad.com/knowledge-base/article/227`.

[44] Mike Glampe. *VFD switching frequency.* (Accessed on 06/02/2021). Oct. 2017. URL: `https://www.kebamerica.com/blog/vfd-switching-frequency/`.

[45] Michael P. Bahrman, Jan G. Johansson, and Bo A. Nilsson. *Voltage Source Converter Transmission Technologies - The right fit for the application.* (Accessed on 06/02/2021). URL: `https://library.e.abb.com/public/b35718ff8f3fa4c0c1256fda004c8ca2/VSC%5C%20TRANSMISSION%5C%20TECHNOLOGIES.pdf`.

[46] Ned Mohan, Tore Undeland, and William P. Robbins. *Power Electronics Converters Applications and Design.* eng. Third. 2002. ISBN: 978-0471226932.

[47] Thomas M. Blooming and Daniel J. Carnovale. *Application of IEEE std. 519-1992 Harmonic Limits.* (Accessed on 06/03/2021). URL: `https://www.eaton.com/content/dam/eaton/products/backup-power-ups-surge-it-power-distribution/power-conditioners/harmonic-correction-unit/IEEE-std-519-1992-harmonic-limits.pdf`.

[48] Kjetil Uhlen and Kamran Sharifabadi. *Communication from supervisors.* (Accessed on 1/2/2020).

[49] Swapnil Yashavant Gadgune. *How to select the split capacitance value in two level three phase inverter?* (Accessed on 06/05/2021). Feb. 2017. URL: `https://www.researchgate.net/post/How-to-select-the-split-capacitance-value-in-two-level-three-phase-inverter?fbclid=IwAR38Jt_stegMMzKSn8ksZYVF2Z7Hg9uCN4eo1dOQJvwl_3kTXPkmr439iE8`.

[50]    Task Force on Harmonics Modeling and Simulation. *Modeling and Simulation of the Propa-gation of Harmonics in Electric Power Networks Part I: Concepts, Models and Simulation Techniques.* (Accessed on 09/11/2020). Jan. 1996. URL: `https://ieeexplore.ieee.org/document/484130`.

[51]    Zhenyu Huang, Yu Cui, and Wilsun Xu. *Application of Modal Sensitivity for Power System Harmonic Resonance Analysis.* (Accessed on 09/11/2020). Jan. 2007. URL: `https://ieeexplore.ieee.org/document/4077113`.

[52]    K.N Md Hasan et al. *An Overview of Harmonic Analysis and Resonances of Large Wind Power Plant.* (Accessed on 10/11/2020). Nov. 2011. URL: `https://ieeexplore.ieee.org/stamp/stamp.jsp?arnumber=6119697`.

[53]    Wilsun Xu et al. *Harmonic Resonance Mode Analysis.* (Accessed on 10/11/2020). June 2005. URL: `https://www.researchgate.net/publication/4155526_Harmonic_Resonance_Mode_Analysis`.

[54]    Henrik Andreas Brantsæter. "Harmonic Resonance Mode Analysis and Application for Offshore Wind Power Plants". (Accessed on 01/12/2020). MA thesis. Norwegian University of Science and Technology, Dec. 2015.

[55]    Atle Rygg. "Impedance-based methods for small-signal analysis of systems dominated by power electronics". (Accessed on 01/03/2021). PhD thesis. NTNU, Oct. 2018.

[56]    Atle Rygg et al. *Frequency-dependent source and load impedances in power systems based on power electronic converters.* (Accessed on 14/03/2020). Aug. 2016. URL: `https://ieeexplore.ieee.org/abstract/document/7540891`.

[57]    PSCAD. *On-Line Frequency Scanner (FFT).* (Accessed on 05/27/2021). URL: `https://www.pscad.com/webhelp/Master_Library_Models/CSMF/On-Line_Frequency_Scanning/fft.htm`.

# Appendix A

# MATLAB-code

This chapter presents parts of the most essential MATLAB-code utilized in achieving the results presented in this thesis. The main script, displayed in Appendix A.1 works as an interface where subsequent scripts can be run, dependent on the frequency range of the analysis. Appendix A.2 presents one of these subsequent scripts.

The main script runs the subsequent scripts dependent on the value of "fstep". The value indicates the frequency increment of the Harmonic Resonance Analysis. All subsequent scripts perform the exact same calculations. Therefore, only the subsequent script where fstep is equal to 10 is displayed.

## A.1 Main script

```matlab
clc
clear all
close all
format long

set(0,'defaulttextinterpreter','latex')
set(0,'defaultlegendinterpreter','latex')

%% Main


fstep = 10;


if fstep == 10
    data_import_fstep10;
    clean_mainmodel_fstep10;
    harmonic_impedance_calc_fstep10;
elseif fstep == 15
    data_import_fstep15hz;
    clean_fstep15hz_data;
    harmonic_impedance_calc_fstep15hz;
elseif fstep == 20
    data_import_fstep20hz;
    clean_fstep20hz_data;
```

```
26          harmonic_impedance_calc_fstep20hz;
27  else
28          data_import_verificationmodel;
29          clean_verification_data;
30          harmonic_impedance_calc_verificationmodel;
31  end
32
33
34
35  %%
36  patch = 0;
37
38  if patch == 1
39          harmonic_impedance_calc_complete;
40  end
```

## A.2    Frequency Step: 10Hz

```
1   %% Defining number of strings
2   n = 1;
3
4   %% Importing data
5
6   if n == 1
7
8       b = dir('*fstep10_grid*.out');
9       outfiles = {b.name};
10      a = natsort(outfiles)';
11
12      fstep10_grid = table();
13      fstep10_grid = table2array(fstep10_grid);
14
15      for i = 1:length(b)
16          filename = a(i);
17          file = load(char(filename));
18          fstep10_grid = cat(2, fstep10_grid, file);
19      end
20
21
22  elseif n == 100
23
24      b = dir('*fstep10_grid_n100*.out');
25      outfiles = {b.name};
26      a = natsort(outfiles)';
27
28      fstep10_grid = table();
29      fstep10_grid = table2array(fstep10_grid);
30
31      for i = 1:length(b)
32          filename = a(i);
33          file = load(char(filename));
```

```matlab
34                    fstep10_grid = cat(2, fstep10_grid, file);
35        end
36
37  end
38
39
40  b = dir('*fstep10_conv*.out');
41  outfiles = {b.name};
42  a = natsort(outfiles)';
43
44  fstep10_conv = table();
45  fstep10_conv = table2array(fstep10_conv);
46
47  for i = 1:length(b)
48          filename = a(i);
49          file = load(char(filename));
50          fstep10_conv = cat(2, fstep10_conv, file);
51  end
52
53
54  if n == 1
55      save('fstep10_data')
56  elseif n == 100
57      save('fstep10_data_n100')
58  end
59
60
61  %% Loading data
62
63  if n == 1
64      load('fstep10_data')
65  elseif n == 100
66      load('fstep10_data_n100')
67  end
68
69  %% Remove time column from each text-file
70
71  % Export1
72  fstep10_grid = array2table(fstep10_grid);
73
74  columnstodelete = [];
75
76  for i = 12:11:width(fstep10_grid)
77      columnstodelete(i) = 1;
78  end
79
80  columnstodelete = columnstodelete';
81  columnstodelete = table(columnstodelete);
82  columnstodelete = columnstodelete.columnstodelete > 0;
83
84  fstep10_grid(:,columnstodelete) = [];
```

```matlab
 85
 86
 87   columnstodelete = [];
 88
 89   % Export2
 90   fstep10_conv = array2table(fstep10_conv);
 91
 92   columnstodelete = [];
 93
 94   for i = 12:11:width(fstep10_conv)
 95       columnstodelete(i) = 1;
 96   end
 97
 98   columnstodelete = columnstodelete ';
 99   columnstodelete = table(columnstodelete);
100   columnstodelete = columnstodelete.columnstodelete > 0;
101
102   fstep10_conv(:,columnstodelete) = [];
103
104   %% Add name for each column in table
105
106   fstep10_grid.Properties.VariableNames(1) = "Time";
107
108   for w = 2:256
109       fstep10_grid.Properties.VariableNames(w) = "V1_ph" + (w-1);
110   end
111
112   for w = 257:511
113       fstep10_grid.Properties.VariableNames(w) = "V1_mag" + (w-256);
114   end
115
116   for w = 512:766
117       fstep10_grid.Properties.VariableNames(w) = "I1_grid_ph" + (w-511)
              ;
118   end
119
120   for w = 767:1021
121       fstep10_grid.Properties.VariableNames(w) = "I1_grid_mag" + (w
              -766);
122   end
123
124
125   %%
126   fstep10_conv.Properties.VariableNames(1) = "Time";
127
128   for w = 2:256
129       fstep10_conv.Properties.VariableNames(w) = "V1_ph" + (w-1);
130   end
131
132
133
```

```matlab
for w = 257:511
    fstep10_conv.Properties.VariableNames(w) = "V1_mag" + (w-256);
end



for w = 1022:1276
    fstep10_conv.Properties.VariableNames(w) = "I1_conv_ph" + (w
        -1021);
end

for w = 1277:1531
    fstep10_conv.Properties.VariableNames(w) = "I1_conv_mag" + (w
        -1276);
end


fstep10_grid_array = table2array(fstep10_grid);
fstep10_conv_array = table2array(fstep10_conv);


%% Determine the mean harmonic magnitudes and phases from the last
    1000 data points, ie. 10ms
for i = 2:256
v1_ph1(i-1) = mean(fstep10_grid_array(length(fstep10_grid_array)
    -1000:end,i));
end
v1_ph1 = v1_ph1';

for i = 257:511
    v1_mag1(i-256) = mean(fstep10_grid_array(length(fstep10_grid_array
        )-1000:end,i));
end
v1_mag1 = v1_mag1';

for i = 512:766
    i1_grid_ph1(i-511) = mean(fstep10_grid_array(length(
        fstep10_grid_array)-1000:end,i));
end
i1_grid_ph1 = i1_grid_ph1';


for i = 767:1021
    i1_grid_mag1(i-766) = mean(fstep10_grid_array(length(
        fstep10_grid_array)-1000:end,i));
end
i1_grid_mag1 = i1_grid_mag1';



for i = 2:256
```

```matlab
178    v1_ph2(i-1) = mean(fstep10_conv_array(length(fstep10_conv_array)
           -1000:end,i));
179    end
180    v1_ph2 = v1_ph2';
181
182    for i = 257:511
183        v1_mag2(i-256) = mean(fstep10_conv_array(length(fstep10_conv_array
               )-1000:end,i));
184    end
185    v1_mag2 = v1_mag2';
186
187
188    for i = 1022:1276
189        i1_conv_ph2(i-1021) = mean(fstep10_conv_array(length(
               fstep10_conv_array)-1000:end,i));
190    end
191    i1_conv_ph2 = i1_conv_ph2';
192
193
194    for i = 1277:1531
195        i1_conv_mag2(i-1276) = mean(fstep10_conv_array(length(
               fstep10_conv_array)-1000:end,i));
196    end
197    i1_conv_mag2 = i1_conv_mag2';
198
199    %% Save
200
201    if n == 1
202        save('clean_mainmodel_data')
203    elseif n == 100
204        save('clean_mainmodel_data_n100')
205    end
206
207    %% Frequency vector
208
209    fstep10 = (100:10:2550)';
210
211    %% Impedance calculation of converter
212
213    for i = 10:length(v1_mag2)
214        Z1_conv_mag_fstep10(i-9) = v1_mag2(i) / i1_conv_mag2(i);
215        Z1_conv_ph_fstep10(i-9) =  v1_ph2(i)  - i1_conv_ph2(i);
216    end
217
218    %% Impedance calculation of grid
219
220    for i = 10:length(v1_mag1)
221        Z1_grid_mag_fstep10(i-9) = v1_mag1(i) / i1_grid_mag1(i);
222        Z1_grid_ph_fstep10(i-9) =  v1_ph1(i)  - i1_grid_ph1(i);
223    end
224
```

```matlab
225  %% Correct the phase if it is above 180 or below -180 degrees
226
227  for i = 1:length(Z1_conv_ph_fstep10)
228      if Z1_conv_ph_fstep10(i) < -180
229          Z1_conv_ph_fstep10(i) = Z1_conv_ph_fstep10(i) + 360;
230      elseif Z1_conv_ph_fstep10(i) > 180
231          Z1_conv_ph_fstep10(i) = Z1_conv_ph_fstep10(i) - 360;
232      end
233
234      if Z1_grid_ph_fstep10(i) < -180
235          Z1_grid_ph_fstep10(i) = Z1_grid_ph_fstep10(i) + 360;
236      elseif Z1_grid_ph_fstep10(i) > 180
237          Z1_grid_ph_fstep10(i) = Z1_grid_ph_fstep10(i) - 360;
238      end
239  end
240
241  %% Equivalent impedance calculation
242
243  for n = 1:length(Z1_conv_mag_fstep10)
244
245      rho_conv = Z1_conv_mag_fstep10(n);
246      theta_conv = Z1_conv_ph_fstep10(n)*pi/180;
247      [real_conv,imag_conv] = pol2cart(theta_conv,rho_conv);
248      Z1_conv = real_conv+imag_conv*1i;
249
250      rho_grid = Z1_grid_mag_fstep10(n);
251      theta_grid = Z1_grid_ph_fstep10(n)*pi/180;
252      [real_grid,imag_grid] = pol2cart(theta_grid,rho_grid);
253      Z1_grid = real_grid+imag_grid*1i;
254
255      Z_eq(n) = 1/( 1/Z1_conv + 1/Z1_grid);
256
257  end
258
259  Z_eq = Z_eq';
260  Z_eq_mag = abs(Z_eq);
261  Z_eq_ph = angle(Z_eq)*180/pi;
262
263  Z_eq = [fstep10,Z_eq_mag,Z_eq_ph];
```